ELSEVIER

Journal of Nuclear Materials 289 (2001) 136–166

journal of nuclear materials

www.elsevier.nl/locate/jnucmat

Alpha-decay damage and aqueous durability of actinide host phases in natural systems

Gregory R. Lumpkin *

Materials Division, Australian Nuclear Science and Technology Organisation, Private Mail Bag 1, Menai, NSW 2234, Australia

Abstract

This paper provides an overview of the geochemical alteration and alpha-decay damage effects observed in the titanate mineral phases brannerite, perovskite, pyrochlore, zirconolite, and the silicate mineral zircon. The available data show that brannerite, pyrochlore, zircon, and zirconolite are all highly durable in natural systems, often surviving the complete destruction of the host rock during weathering. In comparison, perovskite is prone to dissolution and conversion to anatase and other secondary alteration products at moderate to low temperatures. The mineralogical studies provide quantitative data on the crystalline–amorphous transformation and the structure of the metamict state. These studies indicate that the titanate and silicate phases of interest become metamict (amorphous) as a result of the gradual accumulation of alpha-recoil collision cascades. When compared to the data for synthetic pyrochlore and zirconolite doped with ^{238}Pu and ^{244}Cm, dose-age data indicate that the critical dose values for geologically young samples of natural pyrochlore and zirconolite are higher by a factor of approximately 2–3. The available geological data indicate that most of the natural samples occur in rock types that cooled very rapidly to 300°C or lower, followed by slow cooling over geological time periods at lower temperatures without subsequent reheating (metamorphism). Average storage temperatures are on the order of 100–200°C, indicating that the higher critical dose values of the natural samples are due to thermal annealing over geological time periods. The dose-age data also provide evidence for the long-term annealing of isolated alpha-recoil collision cascades in perovskite, pyrochlore, zirconolite, and zircon. Rate constants obtained from the current data sets suggest similar long-term annealing rates of $1–2 \times 10^{-9}$ yr^{-1} for all four minerals. Additional recovery of damage from long-term annealing at ambient conditions will not be significant for time periods up to approximately 10^7 yr.

PACS: 61.16.Bg; 61.50.Ks; 61.80.Jh

1. Introduction

One of the greatest challenges facing scientists, politicians, and the public today is the issue of nuclear waste disposal. In the United States alone, substantial amounts of high level nuclear waste (HLW) have been generated from the operation of commercial nuclear power reactors and by the nuclear weapons program. The combined total volume of HLW in existence at the major facilities in the United States is on the order of 400,000 cubic meters. In addition to this problem, the START I and II Treaties between the United States and the former Soviet Union and Russia present a further challenge as to the dispositioning of plutonium and highly enriched uranium from the dismantling of nuclear weapons. Here again, the quantities are considerable, with approximately 100 metric tons of weapons grade plutonium and several hundred metric tons of enriched uranium [1–3]. Several different types of repositories and wasteform materials have been considered for the disposal of these nuclear wastes, including direct disposal of the unreprocessed spent fuel itself [4–11]. At present, about 17 metric tons of the surplus weapons plutonium are slated for disposal using a pyrochlore-rich titanate ceramic wasteform [12].

* Tel.: +61-2 9717 3475; fax: +61-2 9543 7179.
E-mail address: grl@ansto.gov.au (G.R. Lumpkin).

0022-3115/01/$ - see front matter
PII: S0022-3115(00)00693-0

Advances in wasteform development and testing have been complemented by numerous geological and mineralogical investigations of the analogous crystalline phases in natural environments [13–15]. As pointed out by Ewing [16], one of the most important aspects of nuclear waste disposal is the extrapolation of laboratory data to the long time periods currently required by regulatory agencies for performance assessment (now restricted to a compliance period of 10,000 yr under specific standards for Yucca Mountain [17]). The underlying concept of mineralogical studies is that they can be employed to gain insight into the long-term performance of the ceramic nuclear wasteform under conditions similar to those expected for geological repositories. However, there has been considerable debate over the usefulness of natural analogues in general, particularly in the case of geological systems. For the mineral analogue studies of the kind described in this paper, the degree of correspondence between minerals in their geological environments and laboratory experiments on wasteform phases has received only limited attention [18].

The major titanate mineral phases or groups to be discussed include brannerite, perovskite, pyrochlore, and zirconolite. These phases represent four of the best studied actinide (ACT) and rare earth element (REE) host phases present in the recent polyphase, titanate wasteforms of the type being investigated as part of the Plutonium Immobilization Project (PIP) in the United States. In addition to these phases, the available data for the silicate mineral zircon are also considered. Zircon has also been proposed as a material for the disposal of weapons Pu [19]. Extensive data are also available for the phosphate minerals apatite and monazite, and for baddeleyite (ZrO_2) [20], but a review of these phases is beyond the scope of this paper (see [21] for an overview of natural baddeleyite). Although none of these phases are rock-forming minerals, all of them are important in various types of geological ore deposits as sources of U, Ti, Nb, Ta, and Zr. The principal topics to be covered are the aqueous alteration and radiation damage effects. Several methods of characterization have been used in the study of natural samples, including electron probe microanalysis (EPMA), scanning electron microscopy and microanalysis (SEM–EDX), transmission and analytical electron microscopy (TEM, AEM), X-ray diffraction (XRD), X-ray absorption spectroscopy (EXAFS, XANES), and differential thermal analysis (DTA).

2. Historical perspective

In 1952, even before major concerns arose over the disposal of nuclear wastes, Pabst [22] published an important paper in which he discussed aspects of the metamict (amorphous) state observed in certain minerals. Pabst examined structural aspects of the problem by a comparison of huttonite and thorite, two polymorphs of $ThSiO_4$. The following year, in an important but often overlooked study of natural zircon, Hurley and Fairbairn [23] demonstrated that the mineral experiences a transformation from the crystalline to the metamict state over a finite dose range. Hurley and Fairbairn were among the first researchers to realize to the potential for annealing or recovery of defects induced by alpha-decay damage. The authors also presented an elegant, if somewhat inaccurate, estimate of the number of displaced atoms per alpha-decay event and discussed the radiation damage process in terms of ionization, kinetic energy transfer, and displacement energies! Soon thereafter, the classic study of radiation damage in natural zircons was published by Holland and Gottfried [24], a landmark paper that set the standard for later studies of other mineral analogues and the actinide-doping experiments carried out on synthetic samples. Fundamental issues addressed by Holland and Gottfried included anisotropic unit cell expansion, total volume increases (obtained from density changes), and simple mathematical models relating these and other physical properties and the cumulative alpha-decay dose.

In the mid to late 1970s, considerable interest in alternative wasteforms to borosilicate glass began with the development of supercalcine by McCarthy and coworkers [25,26] and tailored ceramics by Harker and coworkers at the Rockwell International Science Center in the United States (see review by Harker [7]). Ringwood and his colleagues at the Australian National University [27,28] closely followed this work with the initial development phase of Synroc. Ringwood's concept for Synroc called for a material based on minerals that were known, from the geological record, to be highly durable and capable of incorporating the actinides, Sr, Cs, and other fission products present in reprocessed spent fuel. Within two years, Ringwood's group met these criteria by using hollandite, perovskite, and zirconolite as the major phases of the wasteform [29,30]. These developments were followed by some very focused scientific work on natural perovskite and zirconolite samples in support of the development of Synroc [31,32].

During this period, Ewing and co-workers at the Universtiy of New Mexico [33–35] also began to formulate ideas on the application of metamict minerals to the study of ceramic nuclear wasteforms. The development of Synroc and other ceramic nuclear waste forms sparked a 10-yr burst of mineralogical investigations of pyrochlore group minerals, zircon, zirconolite, and other radioactive minerals during the 1980s, primarily involving Ewing's group and co-investigators from Sandia National Laboratories, Los Alamos National Laboratory, and the Boeing Company. Much of this work has continued through the 1990s as part of the Synroc

research and development program at the Australian Nuclear Science and Technology Organisation (ANSTO), with collaborators from Purdue University, The University of New Mexico, and The Natural History Museum (London). Readers interested in the historical development of the mineralogical studies are referred to Ewing [15], who has given a much more detailed review and discussion of the studies noted here, including a description of the work carried out prior to 1950.

3. Chemistry and alteration effects

3.1. Pyrochlore

As described elsewhere [36–38], the structure of pyrochlore is considered to be an anion deficient derivative of the fluorite structure type. Minerals of the pyrochlore group conform to the general formula $A_{2-m}B_2X_{6-w}Y_{1-n} \cdot pH_2O$, where A represents cations in eight-fold coordination, B represents cations in six-fold coordination, and X and Y are anion sites. The A-site accommodates cations of formal valence +1 to +6 and radii from 0.086 to 0.155 nm; whereas, the B-site incorporates cations of formal valence +3 to +6 and radii from 0.060 to 0.083 nm (ionic radii are from Shannon [39]). As a mineral group, the chemistry is extremely diverse, often requiring the analyst to determine 25 or more elements in a single sample [40–48]. Table 1 provides a general list of the elements that can be found on each of the cation and anion sites. As documented here, the structure type is extremely flexible in terms of the sheer number of elements that can be incorporated, and is particularly amenable to the incorporation of actinides [49]. The natural samples are known to contain up to 30 wt% UO_2, 9 wt% ThO_2, and 16 wt% REE_2O_3, an important consideration for the issue of nuclear criticality. However, the crystal chemistry of pyrochlore is not straightforward, owing to the potential for vacancies at the A-, X-, and Y-sites ($m = 0.0$–1.7, $w = 0.0$–0.7, and $n = 0.0$–1.0) and the incorporation of water molecules ($p = 0$–2) in the vacant tunnel sites [50]. The total water content of the natural defect pyrochlores may be as high as 10–15 wt% H_2O.

Prior to the advent of the electron microprobe, most studies of altered natural pyrochlore involved relatively large crystals from laterite zones overlying carbonatite intrusions. These samples tend to be completely altered and are more amenable to wet chemical analysis. In particular, the alteration of pyrochlore in carbonatites to a hydrated, defect pyrochlore enriched in Ba, Sr, or K has been documented in several of the older publications [51–55]. These studies indicate that alteration occurred under low temperature hydrothermal conditions or as a direct result of weathering of the host rock. Subsequently, Van Wambeke [56] and Ewing [57] described the alteration of several complex Nb–Ta–Ti oxide minerals and identified the presence of two distinct types of alteration: primary (hydrothermal) and secondary (due to weathering). Primary alteration resulted in increased Ca concentration; whereas, secondary alteration resulted in hydration and the leaching of REEs and ACTs.

In 1983, Lumpkin and Ewing embarked on a project to understand the crystal chemistry, geochemical alteration, and radiation damage effects of pyrochlore group minerals. Much of the work relied on the development of analytical procedures and the procurement of suitable standards for EPMA. Based on a limited number of samples, this work showed that primary alteration resulted in decreased Na contents, minor increases in Mn and Fe, and variable to minor changes in Ca, F, H_2O, and A-site vacancies. Secondary alteration resulted in leaching of Na, Ca, F, extensive hydration, and cation exchange for large cations like K, Sr, Ba, Pb, and Cs [58]. Further results were published as part of a major study of the mineralogy and radiation damage effects of Ta-rich pyrochlore (microlite) samples from the Harding pegmatite in northern New Mexico. In this work, Lumpkin et al. [45] demonstrated that major increases in Ca, Mn, and O occurred at the expense of Na, F, and vacancies as a result of primary, hydrothermal alteration. The Harding samples were found to exhibit minor secondary alteration localized along fractures in the microlite crystals. For this type of alteration, chemical changes inferred from the EPMA data indicated a major depletion of Na, F, Ca, and O in the altered areas, compensated by increased vacancies, major hydration (8–13 wt% H_2O) and minor increases in the Mn and Fe content.

Following the work on the Harding microlites, additional results on the alteration of microlite were reported in two other studies. Wise and Cerny [46] analyzed a suite of microlite samples from the Canadian Yellowknife pegmatite field and concluded that hydro-

Table 1
A summary of the chemical composition of natural pyrochlore

Site	Major elements	Minor elements
A (16c)	Na, Ca, REE, Th, U^{4+}, U^{6+}	K, Sr, Sb^{3+}, Sn^{2+}, Cs, Ba, Pb, Bi
B (16d)	Nb, Ta, Ti, Zr, Sn^{4+}	Mg, Al, Mn, Fe, Sb^{3+}, W
X (48f)	O	OH
Y (8a)	O, OH, F, H_2O	K, Cs

thermal alteration of the samples caused progressive losses of Na, Ca, and U, with increased vacancies and hydration. In a study of microlite from the Beauvoir granite, France, Ohnenstetter and Piantone [48] documented late stage leaching of Na, Ca, and F in selected samples. Hydration and minor increases in K and Pb accompanied the documented elemental losses. Furthermore, the alteration appeared to be largely confined to U-rich cores of the crystals, suggesting an enhanced alteration of the more heavily radiation-damaged microlite. This is perhaps the first direct evidence for a radiation damage enhanced leaching mechanism in pyrochlore.

Lumpkin and Ewing [59–61] concluded their studies of alteration in pyrochlore group minerals with the publication of three papers from 1992 to 1996 dealing with the microlite, pyrochlore, and betafite subgroups. These results are summarized below and in Table 2. Examples of the alteration are shown in Fig. 1. In addition to the usual primary and secondary alteration types, an intermediate stage of alteration was identified in a few samples and was referred to as transitional alteration [60]. Primary alteration patterns are depicted graphically in Fig. 2. The alteration vectors of microlite and U-rich pyrochlores from granitic pegmatites are consistent with formal substitution schemes such as $^{A}\square^{Y}\square \rightarrow {}^{A}Ca^{Y}O$, $^{A}Na^{Y}F \rightarrow {}^{A}Ca^{Y}O$ (where $\square$ represents a vacancy). The substitution $^{A}Na^{Y}OH \rightarrow {}^{A}Ca^{Y}O$ was inferred for the cases where there are only minor changes in the F content were evident from EPMA, but there was little evidence for the simple substitution $^{Y}F \rightarrow {}^{Y}OH$. Some samples from carbonatites and nepheline syenite pegmatites were found to have primary alteration patterns indicating a leaching process, e.g., $^{A}Na^{Y}F \rightarrow {}^{A}\square^{Y}\square$, and $^{A}Ca^{Y}O \rightarrow {}^{A}\square^{Y}\square$.

Transitional alteration was only observed in certain samples of the pyrochlore subgroup, including U-rich pyrochlore from granitic pegmatites and Na–Ca pyrochlores from carbonatites and nepheline syenite pegmatites. EPMA of unaltered and altered areas of these samples are consistent with a substitution of the form $^{A}Na^{Y}F \rightarrow {}^{A}\square^{Y}\square$. The salient feature of transitional alteration is loss of Na and F combined with some cation exchange for Sr, Ba, REE, and Fe to produce a hydrated pyrochlore near $AB_2O_6 \cdot H_2O$ in stoichiometry (Fig. 2).

Secondary alteration trends are consistent with the substitution schemes $^{A}Ca^{Y}O \rightarrow {}^{A}\square^{Y}\square$, $^{A}Na^{Y}F \rightarrow {}^{A}\square^{Y}\square$, and $^{A}Ca^{X}O \rightarrow {}^{A}\square^{X}\square$. The structural formulae of these samples exhibit extreme numbers of A-site, Y-site, and X-site vacancies ranging up to maximum values of 1.7, 1.0, and 0.7 per formula unit, respectively (Fig. 2). These defect pyrochlores typically contain up to 10–15 wt% H_2O. This style of late, fracture-controlled alteration or leaching can be found in pyrochlores from all of the major host rock categories, commonly cutting across earlier primary or transitional alteration. Major cation exchange effects are normally limited to pyrochlores found in lateritic environments (e.g., Ba pyrochlore from Araxá, Brazil, and the K–Sr pyrochlores from Lueshe, Zaire). Detailed descriptions of the transformation of primary Na–Ca pyrochlore to the various hydrated, defect pyrochlore compositions during weathering of these deposits are given elsewhere [62–64].

A variety of alteration effects have been observed in completely metamict samples of the Ti-rich betafite subgroup. In two samples from Canada with ages of 1000 Ma, Lumpkin and Ewing [61] concluded that the major result of alteration was hydration, with only minor changes in elemental composition. However, many other natural betafites exhibit relatively low temperature, secondary alteration that initially proceeds by leaching of Na, Ca, and F. The alteration is usually accompanied by hydration together with minor increases in Al, K, Mn, Fe, Sr, and Ba. At this stage, U and Th remain relatively unaffected by the alteration process (stage 1). This stage of alteration can be modelled by the following reaction:

$$2.5H^{+} + H_2O + CaNa_{0.5}U_{0.5}TiNbO_{6.5}F_{0.5} \rightarrow U_{0.5}TiNbO_{5.5} \cdot 2H_2O + Ca^{2+} + 0.5Na^{+} + 0.5HF \quad (1)$$

Once Na and F are removed and the Ca content drops below about 0.2–0.3 atoms per formula unit (~2.5–3.5 wt% CaO), betafite bulk compositions fall within the stability field of liandratite + uranpyrochlore + rutile (or anatase), thus promoting major element mobility (including Th, U, Pb, and B-site cations), incipient recrystallization, and partial dehydration (stage 2). The

Table 2
Geochemical alteration effects in natural pyrochlore

Alteration type	T (°C)	Elements lost	Elements gained
Primary P1	350–650	Na, F	Ca, O, Mn, Fe
Primary P2	300–550	Na, F, Ca, O, Pb	Fe, Sr, H_2O
Transitional	200–350	Na, F, Pb	Fe, Sr, Ba, REE, H_2O
Secondary (a)	<100	Na, F, Ca, O	Mn, Fe, Cs, Ba, REE, H_2O
Secondary (b)	<150	Na, F, Ca, O, Pb	K, Fe, Sr, Ba, REE, Pb, H_2O

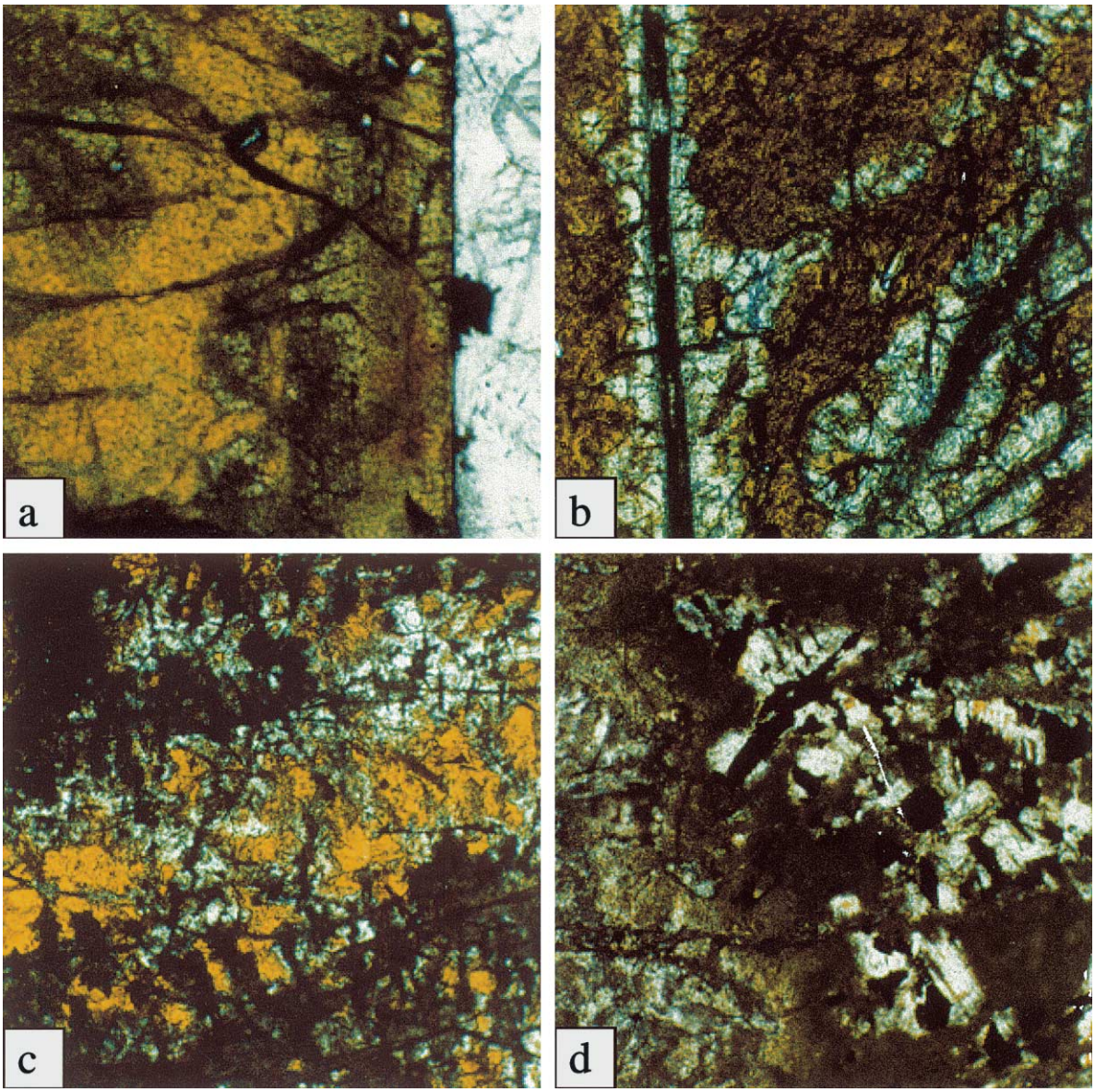

Fig. 1. Optical micrographs of alteration in pyrochlore group minerals. (a) Primary, hydrothermal alteration of pyrochlore from carbonatite, Alnö, Sweden ($t = 537$ Ma). Unaltered interior zone is yellow in color. (b) Typical fracture controlled secondary alteration of metamict U-rich pyrochlore, Ontario, Canada ($t = 1000$ Ma). (c) Secondary alteration (stage I) of metamict betafite, Madagascar ($t = 500$ Ma). Unaltered betafite is yellow in color, surrounded by colorless and dark alteration zones. (d) Secondary alteration (stage II) in the rim of a metamict betafite crystal, Madagascar. Alteration assemblage consists of rutile (black), a secondary pyrochlore phase (white), and liandratite (gray rims on pyrochlore). Field of view in each image is approximately 0.5 mm.

breakdown of leached betafite was modeled according to three idealized reactions of the form:

$$2U_{0.5}TiNbO_{5.5} \cdot 2H_2O \rightarrow UNb_2O_8 + 2TiO_2 + 3H_2O + 2H^+ + 2e^- \quad (2)$$

$$4U_{0.375}TiNbO_{5.25} \cdot 2H_2O \rightarrow UNb_2O_8 + U_{0.5}Nb_2O_{6.5} \cdot H_2O + 4TiO_2 + 5.5H_2O + 3H^+ + 3e^- \quad (3)$$

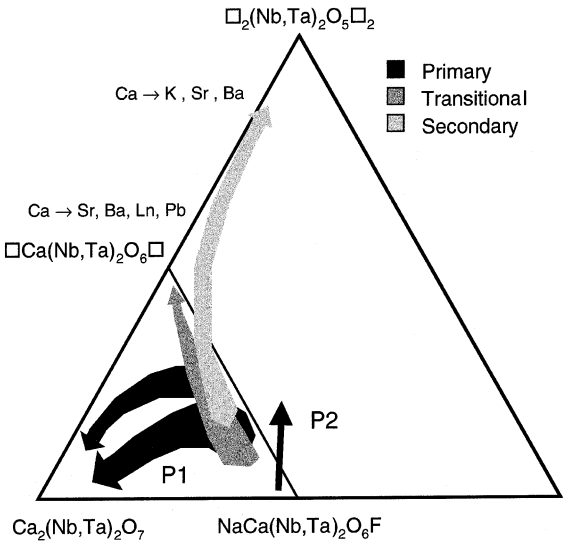

Fig. 2. Schematic representations of alteration effects in pyrochlore group minerals. Major trends are shown for primary (hydrothermal, $T \sim 300$–500°C), transitional (hydrothermal, $T \sim 100$–350°C), and secondary (near surface and weathering, $T < 150$°C) alteration. Replacement of Ca by large cations is common in the defect pyrochlores, particularly near the join between $\square Ca(Nb,Ta)_2O_6\square$ and $\square_2(Nb,Ta)_2O_5\square_2$.

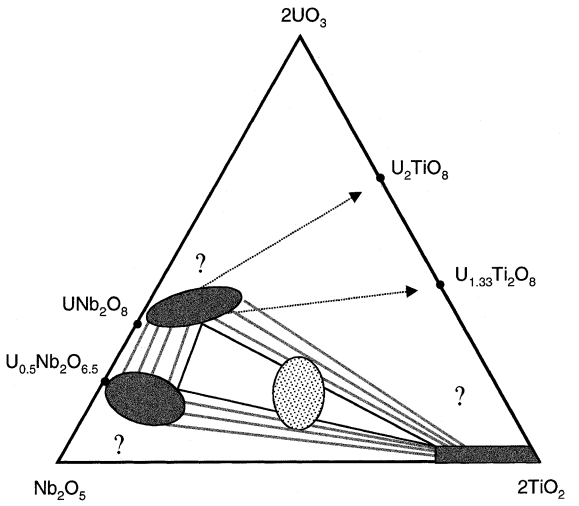

Fig. 3. Schematic representations of the alteration of betafite under near surface, oxidizing conditions. Stage 1 follows the secondary trend shown in Fig. 2. This figure depicts the breakdown of betafite during stage 2 of secondary alteration, after leaching of Na, F, and most of the Ca during stage 1. Initial betafite compositions project within the stippled area. The dark shaded areas represent the compositions of the alteration products liandratite (ideally UNb_2O_8), secondary pyrochlore (ideally $U_{0.5}Nb_2O_{6.5}$), and rutile or anatase (ideally TiO_2).

$$2U_{0.25}TiNbO_5 \cdot 2H_2O \rightarrow U_{0.5}Nb_2O_{6.5} \cdot H_2O + 2TiO_2 + 2.5H_2O + H^+ + e^- \quad (4)$$

The alteration observed in betafite samples from Madagascar is illustrated schematically in Fig. 3. In three out of four samples, no loss of U or Th was observed. However, in the fourth sample up to 20–30% of the original amount of U was lost during the secondary alteration and recrystallization of the amorphous betafite. Part of this U is retained by liandratite crystallized in the adjacent host rock [61].

Lumpkin and Mariano [62] have also described another instance of U loss during alteration. In this work, EPMA results for samples from Mountain Pass, California, provide evidence for the hydrothermal alteration of uranpyrochlore to plumbopyrochlore in a carbonate-rich environment. The alteration resulted in major increases in Pb and Si, and minor increases in Al and F at the expense of Ca, Fe, U, Nb, and O. The unaltered areas of the pyrochlore grains typically contain 17–24 wt% UO_2; whereas, the altered areas contain 7.2–15 wt% UO_2, consistent with loss of approximately 11–70% of the U. The Si is positively correlated with Al and together they exhibit a good negative correlation with Nb and Ti and a good positive correlation with Pb and Sr at the A-site. The role of Si in these and other radiation-damaged samples is a topic for further research (see [62] for further details).

An important new occurrence of betafite has recently been described by Lumpkin et al. [65] in 42 Ma hydrothermal vein samples from Adamello, Italy. The betafite occurs as overgrowths on zoned zirconolite grains and contains 29–34 wt% UO_2. In terms of end-members, betafite contains approximately 50 mole percent $CaUTi_2O_7$ and is the closest known natural composition to the pyrochlore phase proposed for use in titanate waste forms. Detailed electron microscopy and microanalysis showed that these betafites have only suffered a minor late stage hydration event as evidenced by lower backscattered electron image contrast around the rims of the grains. Except for lower totals, electron probe data revealed little difference in composition between the altered rims and unaltered areas, consistent with simple hydration. This is also shown pictorially in Fig. 4 by inspection of the SEM image and corresponding X-ray maps. Results of this study demonstrate quantitative retention of U and Th for time periods of 40 Ma, even though the cumulative total alpha-decay dose is on the order of 3–4×10^{16} α mg^{-1}.

3.2. Zirconolite

The structure of zirconolite is also considered to be an anion deficient derivative of the fluorite structure

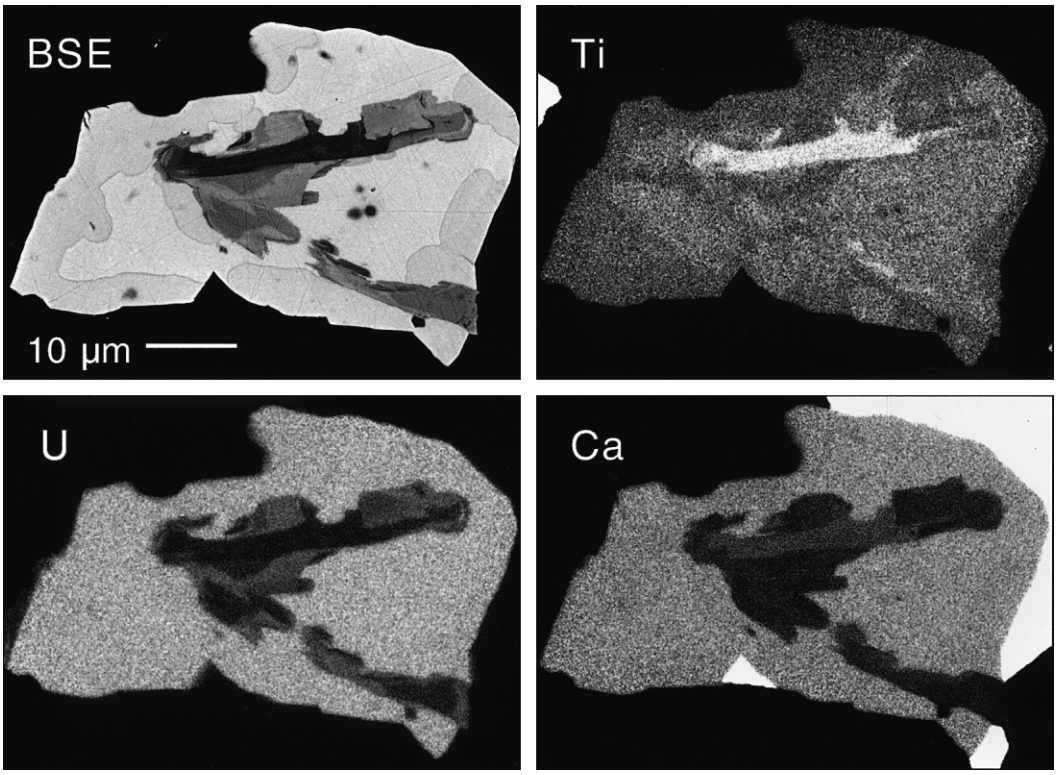

Fig. 4. SEM backscattered electron image and X-ray maps of a betafite overgrowth on zirconolite, Adamello, Italy ($t = 42$ Ma). The backscattered (BSE) image shows partial replacement of zoned zirconolite by betafite and late stage alteration of the betafite rim (slightly darker contrast). Note that zirconolite was not affected by alteration. The accompanying Ti, U, and Ca X-ray maps show that these elements were not affected by the alteration. Variation of Ti in betafite is due to original compositional zoning (e.g., $2Ti = Nb + W$) of B-site cations. Detailed analyses indicate that the alteration mainly involved hydration of the betafite.

type [62–69]. Furthermore, zirconolite can be visualized as a volumetrically condensed, layered version of pyrochlore with reduced symmetry [38,70]. Ideally, the chemical composition of zirconolite is $CaZrTi_2O_7$, but in nature it commonly deviates from this end-member composition due to extensive substitution primarily on the Ca- and Ti-sites [71–77]. In the structure of zirconolite-2M, the monoclinic aristotype, the Ca-site is eight coordinated and is occupied by cations of formal valence +2 to +4 with ionic radii from 0.096 to 0.1143 nm. There are three distinct Ti sites in zirconolite-2M which accommodate cations of formal valence +2 to +6 with radii ranging from 0.0535 to 0.083 nm. The Zr-site is seven coordinated, but in natural samples this site is subject to only limited substitution by other elements (see [78,79] for recent reviews of the chemistry and substitution mechanisms). Table 3 gives a list of the elements that substitute for Ca, Zr, and Ti, demonstrating that natural zirconolite can be as chemically complicated (and as difficult to analyze) as their pyrochlore cousins. More importantly, the natural zirconolites demonstrate the ability to incorporate up to 24 wt% UO_2, 22 wt% ThO_2, and 32 wt% REE_2O_3 in the structure.

In constrast to pyrochlore, only limited amounts of data exist on the alteration of zirconolite in natural systems. Oversby and Ringwood [32] have previously demonstrated that zirconolite has remained a closed system to U, Th, and Pb for up to 650 Ma. These authors showed that 10 samples from Norway, Russia, Sri Lanka, and Brazil gave concordant $^{206}Pb/^{238}U$,

Table 3
A summary of the chemical composition of natural zirconolite

Site	Major elements	Minor elements
M8	Ca, REE (La–Nd), Th, U	Mn, Sr
M7	Zr	Ti, REE (Sm–Lu), Hf, U
M5,6	Ti, Mg, Fe^{2+}, Fe^{3+}, Nb	Al, Cr, Mn, Zn, Ta, W

$^{207}Pb/^{235}U$, and $^{206}Pb/^{207}Pb$ isotopic ages. One polyphase sample from Sri Lanka was found to be slightly discordant, possibly to due loss of about 9% of the radiogenic Pb. Another sample obtained from weathered rock at Jacupiranga, Brazil, appeared to have lost approximately 13% of the radiogenic Pb. In both cases where loss of radiogenic Pb was postulated, the samples had unusually high common Pb contents leading the authors to an alternative explanation involving the presence of a second phase rich in the common Pb component. Most importantly, none of the samples showed evidence for U loss. These results were obtained in spite of the fact that many of the samples are completely amorphous due to alpha-decay damage (doses of up to 1.1×10^{17} α mg^{-1} were reported). Furthermore, the samples from Sri Lanka occur in stream gravel deposits having survived the complete breakdown of the host rock during weathering.

Following this work, Ewing et al. [80] reported EPMA data for several zirconolite samples from Sri Lanka and Phalaborwa, South Africa. XRD work showed that all of these zirconolites were completely metamict. EPMA results for the Sri Lanka samples demonstrated that there is a general lack of alteration at the 1 μm scale of probe resolution, with the exception of a slight decrease in the ThO_2 content and slightly lower analytical totals in the rims of the grains. The authors also suspected some alteration of the Phalaborwa sample from the low cation total of 3.89 and very low Ca-site total of 0.77 based on 7.00 oxygens. Furthermore, TEM studies revealed the presence of some microcrystalline domains in the sample, possibly related to the alteration event.

The first report of the corrosion of zirconolite at relatively high temperature and pressure in a hydrothermal system was published by Gieré and Williams [74] in 1992. During their study of the mineralogy and petrology of Ti-rich veins from the Adamello contact aureole of northern Italy, zirconolite was discovered in two-vein zones, the phlogopite zone and the titanian clinohumite zone. The authors only found evidence for the corrosion of zirconolite in the phlogopite zone. In these strongly zoned zirconolites, the initial growth stages were followed by a period of corrosion and replacement by a new generation of zirconolite, resulting in a major decrease in the concentrations of Th and U. A second period of corrosion led to the formation of REE and Nb enriched rims on the zirconolite grains. Thermodynamic analysis of the mineral assemblages indicated that the zirconolite-bearing vein zones crystallized at 500–600°C from a reducing hydrothermal fluid phase. This fluid was rich in H_2S, HCl, HF, and P and relatively poor in CO_2 [73]. Recent work has also shown that certain zirconolite grains in the titanian clinohumite zone exhibit some corrosion and replacement features in association with overgrowths of betafite [65] (see Fig. 4(a)). However, there is no evidence for low temperature alteration of these zirconolites either from microscopy studies or from studies of the U series isotope systematics [81]. Replacement of zirconolite by zircon, sphene, and rutile has also been documented in metamorphosed ferromagnesian silicate rocks at Manitouwadge, Canada [82]. In this case, the corrosion and replacement of zirconolite occurred at a temperature above 600°C in the presence of a regional metamorphic aqueous fluid phase.

Lumpkin, Gieré, and co-workers [83,84] have described the alteration of metamict zirconolite from the 2060 Ma carbonatite complex of Phalaborwa, South Africa. As shown in Fig. 5, the alteration follows microfractures and resulted in the incorporation of Si and loss of Ti, Ca, and Fe, but the Th and U content

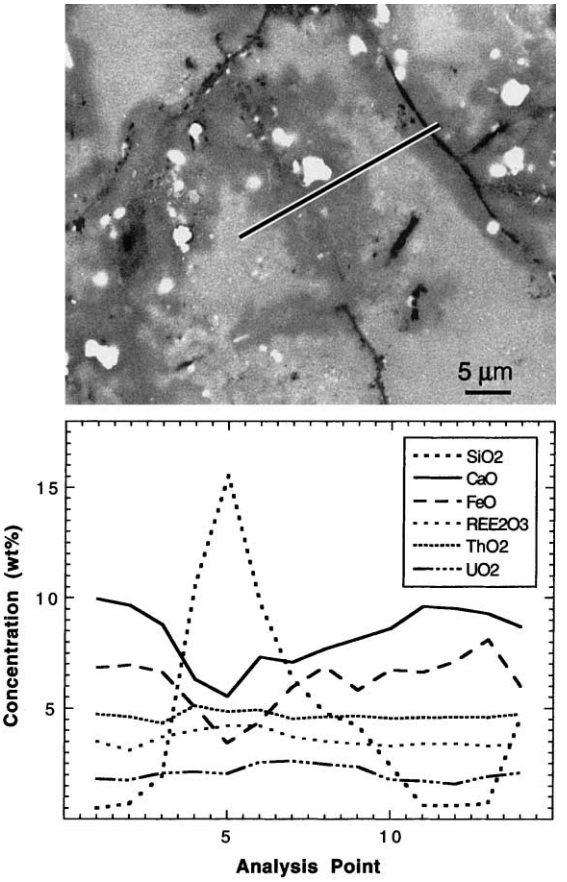

Fig. 5. BSE image and EPMA profiles of alteration in zirconolite from Phalaborwa, South Africa ($t = 2060$ Ma). The backscattered image shows alteration as darker areas along cracks. White spots are galena, possibly formed in part from radiogenic Pb. EPMA analyses taken along the line marked on the BSE image show a major increase in Si and decrease in Ca and Fe in the altered zones; whereas, the REEs, Th, and U remain relatively constant.

Table 4
Geochemical alteration effects in natural zirconolite

Alteration type	T (°C)	Elements lost	Elements gained
Replacement	620–680	(breakdown to zircon + titanite + rutile)	
Corrosion-replacement	500–600	Mg, Fe, Th, U	Ti, Ca
Hydrothermal	<400–500	Ca, Ti, Fe, Pb	Si, H_2O
Hydrothermal	<400–500	Ca, Fe	Si, H_2O
Hydrothermal	<400–500	Ca, Fe	Si, Ti, Zr, REE, H_2O

remained relatively constant. Radiogenic Pb appears to have been mobile and precipitated mainly within the altered areas as galena (PbS). Unfortunately, the conditions under which the alteration occurred are not well constrained. More recently, Bulakh et al. [76] described the alteration of zirconolite (referred to as zirkelite in their paper) from the Sebl'yavr carbonatite complex, Russia. In this example, the zirconolite has been pseudomorphed and replaced along cracks by an unidentified Ba–Ti–Zr–Nb silicate phase. Additional evidence for geochemical alteration has been found in two other zirconolite samples (C.T. Williams, personal communication). In both cases, the alteration is similar to that of the Phalaborwa and Sebl'yavr samples and involves increased Si and/or replacement by a silicate mineral phase. These observations point to the potential instability of zirconolite in the presence of hydrothermal fluids rich in Si. Selected images are presented in Fig. 3 to illustrate the alteration of zirconolite in natural systems. The available data are summarized in Table 4 to illustrate the alteration of zirconolite in natural systems.

3.3. Perovskite

Perovskite is an ABX_3 structure type based around a framework of corner sharing, octahedral B-site cations [38,85]. The large A-site cations occupy the center of a large cavity formed by eight B-site octahedra and are coordinated to 12 oxygens in the ideal cubic structure. In reality, most perovskites are distorted via octahedral tilting and generally have lower symmetry. In nature, only near end-member $SrTiO_3$ is cubic, most other compositions are orthorhombic. Mitchell [85] has shown that most natural perovskites can be described in the quaternary system defined by the end-members $CaTiO_3$ (perovskite), $(Na_{0.5}REE_{0.5})TiO_3$ (loparite), $NaNbO_3$ (lueshite), and $SrTiO_3$ (tausonite). Natural samples generally exhibit complete solid-solution along the perovskite–loparite join and near the loparite–tausonite join. Additional end-members found in natural samples include $Ca(Nb_{0.5}Fe^{3+}_{0.5})O_3$ (latrappite), and the postulated non-stoichiometric layered compounds $Ce_2Ti_2O_7$ and $Ca_2Nb_2O_7$ [85]. Many modern EPMA results are now available for perovskite samples obtained from different geological environments [86–93]. The available chemical data indicate that the major A-site cations in natural perovskites are Na, Ca, Sr, and REE (La–Nd), with minor amounts of K, REE (Sm–Gd), Ba, and U. In most samples, Th is usually a minor constituent, but concentrations up to 18.4 wt% ThO_2 have been reported in perovskite from the Khibina alkaline complex, Russia [89]. Ti, Fe, and Nb, and minor quantities of Mg, Al, Zr, and Ta primarily occupy the B-site.

Shortly after Ringwood and co-workers proposed Synroc as a wasteform, Nesbitt et al. [94] investigated the thermodynamic stability of perovskite. Using the available thermochemical data, these authors calculated that sphene ($CaTiSiO_5$) is thermodynamically stable relative to perovskite (end-member $CaTiO_3$) in the presence of silicate minerals, including quartz, feldspar, pyroxene, and kaolinite. Additional calculations showed that rutile, sphene, calcite, and quartz are stable relative to perovskite in many natural ground waters and hydrothermal fluids up to temperatures of 300°C. This appears to be borne out by studies of perovskite in near surface environments. For example, Mariano [95] has reported that major economic deposits of Ti occur in Brazil within laterite horizons above carbonatite host rocks where near end-member perovskite has been completely altered to anatase, cerianite, monazite, or minerals of the crandallite group during weathering. In a study of altered perovskite from one of these localities, Banfield and Veblen [96] proposed that the perovskite–anatase reaction mechanism involves topotactic inheritance of layers of the perovskite Ti–O framework. There is at least some evidence in the geological literature to suggest that solid-solution toward $Ca(Nb_{0.5}Fe^{3+}_{0.5})O_3$ may improve the durability of perovskite [97].

Mitchell and Chakmouradian [91] have recently reported on the instability of near end-member perovskites under hydrothermal conditions in carbonatite (Sebl'yavr, Russia) and kimberlite (Iron Mountain, Wyoming) host rocks. The alteration probably occurred at temperatures of approximately 250–300°C and 500–600°C, respectively. In these examples, the perovskite was replaced by kassite, anatase, titanite, calcite, and ilmenite in the presence of a CO_2- and SiO_2-rich fluid phase. Several mineral reactions were postulated to explain the observations:

$$2CaTiO_3 + CO_2 + H_2O \leftrightarrow CaTi_2O_4(OH)_2 + CaCO_3 \quad (5)$$

$$CaTiO_3 + CO_2 \rightarrow TiO_2 + CaCO_3 \quad (6)$$

$$CaTi_2O_4(OH)_2 + CO_2 \rightarrow 2TiO_2 + CaCO_3 + H_2O \quad (7)$$

$$CaTi_2O_4(OH)_2 + SiO_2 \rightarrow 2TiO_2 + CaTiSiO_5 + H_2O \quad (8)$$

$$TiO_2 + 2Fe^{2+} + 2H_2O \rightarrow 2FeTiO_3 + 4H^+ \quad (9)$$

Reactions (5) and (6) describe the initial breakdown of perovskite during progressive leaching of Ca. The early alteration product kassite continued to react with the fluid phase to produce a later generation of anatase, more calcite, and some titanite according to reactions (7) and (8). Ilmenite was one of the final alteration products and formed from the breakdown of anatase as described by reaction (9). The instability of perovskite shown here is consistent with the earlier work of Nesbitt and coworkers [94].

Recent work has also demonstrated that perovskites dominated by the loparite component are subject to alteration in hydrothermal fluids. Lumpkin et al. [98] examined a small suite of perovskite samples covering a range of compositions and found that those from fresh rock are generally pristine and unaltered. However, alteration was observed in a loparite sample from a nepheline syenite pegmatite near Bratthagen, Norway. The altered perovskite crystal is shown in Fig. 6. Analytical electron microscopy indicated that the alteration resulted in nearly complete leaching of Na from the A-site and uptake of minor amounts of Al and Si (0.1–0.2 wt% Al_2O_3, 1.1–1.8 wt% SiO_2). Analyses of unaltered and altered areas of the sample revealed that the contents of most other elements are essentially unchanged, including the lanthanides. Based on these data, the following reaction was proposed:

$$0.5H^+ + Na_{0.5}REE_{0.5}TiO_3 \rightarrow \square_{0.5}REE_{0.5}TiO_{2.5}(OH)_{0.5} + 0.5Na^+ \quad (10)$$

Alteration of the loparite probably occurred during late stage alteration of the host rock which produced zeolites, clay minerals, diaspore, gibbsite and other minerals at temperatures below approximately 300–400°C. This mechanism of Na leaching and hydrogen ion exchange, accompanied by minor changes in Ca and Sr, was also reported by Chakhmouradian et al. [93] in loparite from the Burpala alkaline complex, Russia. At Burpala, the alteration probably occurred at a temperature below 400–500°C. In both occurrences, the alteration product (metaloparite) is metamict; whereas, the unaltered loparite is moderately to highly crystalline (see Section 4.3). The reports cited here provide confirmation of previous work on 'metaloparite' from the Lovozero complex, Russia (see [85]). Metaloparite from Lovozero contains

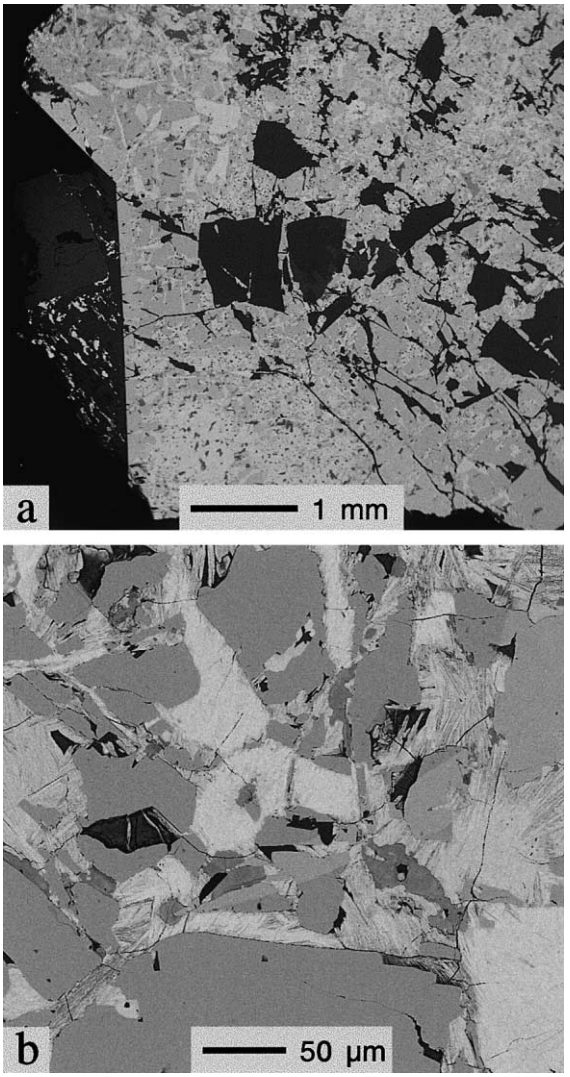

Fig. 6. Backscattered electron images of altered perovskite (loparite) from Bratthagen, Norway ($t = 295$ Ma). (a) Low magnification view showing a large part of the crystal and its alteration products, including metaloparite (light) and analcime (dark). (b) Higher magnification image showing loparite (medium gray) and metaloparite (light). The lighter contrast of the alteration phase is due to the nearly complete leaching of Na.

3.49 wt% H_2O and only 0.23 wt% Na_2O. By way of comparison, calculations for charge balance by OH gave estimated H_2O contents of 2.2–2.4 wt% for the altered loparite from Bratthagen, although higher total water contents are possible if H_2O molecules occupy vacant A-sites [96].

3.4. Brannerite

Brannerite, ideally UTi_2O_6, has a crystal structure based on a distorted array of hexagonal close packed

oxygens. The structure consists of layers of Ti octahedra connected by columns of U octahedra [99]. These structural elements have features in common with anatase and rutile, respectively. Recent investigations have shown that both synthetic [100] and natural brannerites [1 0 1] can incorporate substantial amounts of Ca, REE, Th, and other elements. In both cases, the incorporation of lower valence elements on the A-site may be charge balanced by oxidation of some U^{4+} to U^{5+} and/or U^{6+} ions. This is supported by several of the wet chemical analyses reported previously [102–104]. For example, of six analyses in which both UO_2 and UO_3 were determined, five have $UO_2/(UO_2 + UO_3)$ weight ratios of 0.20, 0.24, 0.32, 0.48, and 0.90. The sixth sample only had a trace of UO_2 reported in the analysis. Using a small suite of samples from different localities, Lumpkin et al. [101] have shown that unaltered brannerite can contain up to 1.2 wt% Al_2O_3, 2.3 wt% SiO_2, 7 wt% CaO, 0.6 wt% MnO, 2.6 wt% FeO, 0.7 wt% NiO, 4.2 wt% Y_2O_3, 1.8 wt% Nb_2O_5, 3.5 wt% REE_2O_3, 7 wt% PbO, and 15 wt% ThO_2.

The SEM–EDX and TEM studies carried out by Lumpkin et al. [101] revealed that the natural brannerite samples exhibit a range of alteration, from relatively unaltered to highly altered. Examples of the alteration are shown in Fig. 7. In the early stages, the alteration is usually confined within irregular patches, narrow veinlets, or around the rim of the sample. At an advanced stage of alteration, a large proportion of the brannerite is affected and other secondary phases may be present, including anatase, galena, and thorite. The altered areas of the brannerites have U contents as low as 1 wt% UO_2 and elevated Ti contents, ranging up to 82 wt% TiO_2. Additional constituents that may be enriched in the altered areas include up to 6.3 wt% P_2O_5, 7.0 wt% As_2O_5, 18 wt% SiO_2, 5.9 wt% Al_2O_3, and 16 wt% FeO. These results demonstrate that up to 95% (by weight) of the original amount of UO_2 was lost as a result of alteration. Fig. 8 illustrates the relationship between U loss and the incorporation of Si from the attending fluid phase.

Another important result of this work is the observation of microfracturing of the associated rock matrix or intergrown mineral phases. This has been documented in three brannerite samples. In two cases where the brannerite grains showed alteration, the associated microfractures are filled with a poorly characterized U-rich secondary material, consistent with the quantitative evidence for U loss presented above. These results imply that local transport of U away from the source brannerite occurred during alteration under relatively oxidizing conditions suitable for the formation of uranyl complexes in the fluid phase.

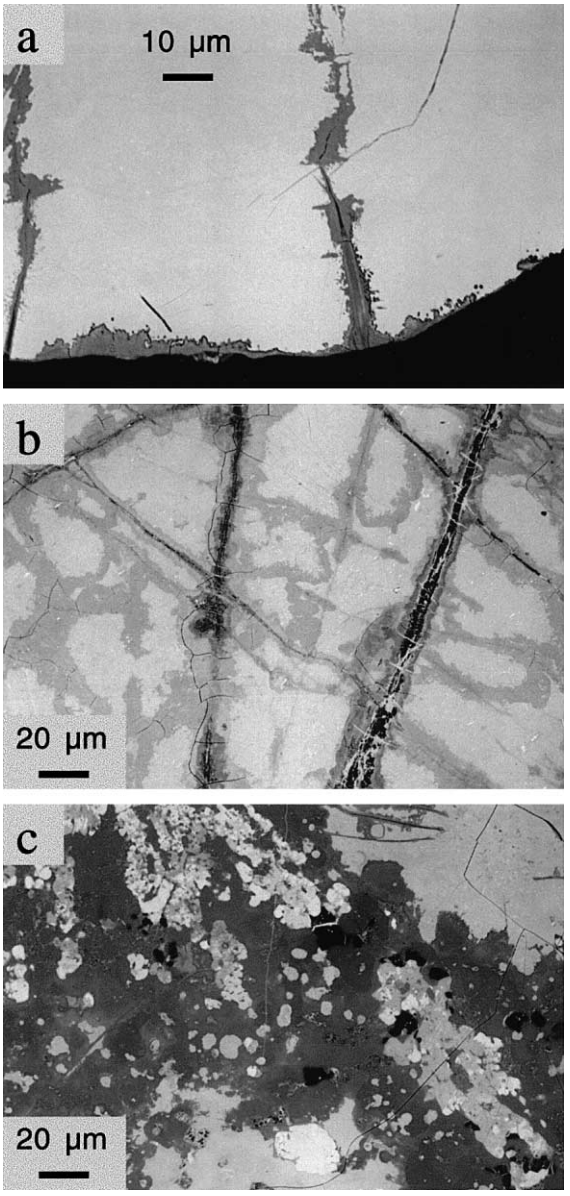

Fig. 7. BSE images of brannerite. (a) Relatively unaltered material from Ticino, Switzerland ($t = 20$ Ma). Note minor alteration (darker gray) along the rim and microcracks. (b) Moderately altered brannerite from Cordoba, Spain ($t = 400$ Ma), showing typical fracture control. (c) Heavily altered brannerite from Crocker's Well, South Australia ($t = 1580$ Ma), showing the secondary phases thorite (lightest gray) and anatase (black). Altered brannerite (darker gray levels) has lost U and gained Si (see Fig. 8).

3.5. Zircon

Zircon, ideally $ZrSiO_4$, is a common accessory mineral found in a variety of geological environments. Zircon is classified as an orthosilicate due to the presence of isolated SiO_4 tetrahedra, but the structure actually consists of a framework of edge sharing silicate tetrahedra and eight coordinated Zr-sites [105]. In

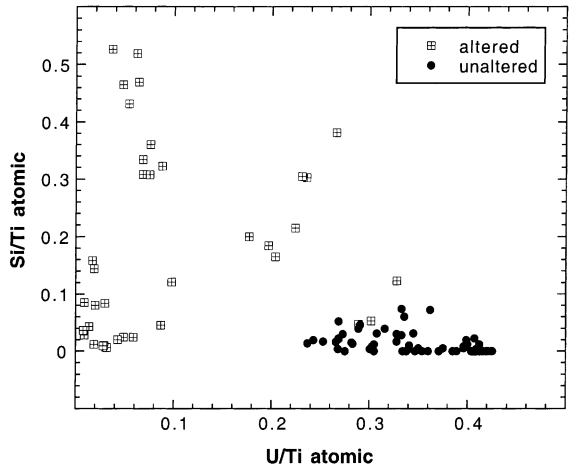

Fig. 8. Plot of the atomic ratio of Si/Ti versus atomic U/Ti for unaltered and altered areas of natural brannerite. Note the severe U loss and incorporation of large amounts of Si in the altered brannerite.

general, the major elemental impurity is Hf, which substitutes for Zr and can be the dominant cation on this site in highly fractionated granitic pegmatites. Trace to minor amounts (generally 5000 ppm or less) of other elements may be present, including Ca, REE, Th, and U on the Zr-site and P on the Si-site. All of these elements may be enriched significantly, especially in zircon specimens from granitic pegmatites. Maximum concentrations of approximately 26 wt% REE_2O_3, 10 wt% ThO_2, 10 wt% UO_2 and 5 wt% CaO have been reported in zircon, but these values are exceptional. Natural zircons have also been reported to contain substantial total water contents and the available evidence indicates that both OH^- and H_2O species may be present [105,106]. Aines and Rossman [106] have suggested that small amounts of water (as OH^-) are incorporated by radiation-damaged zircon as a means of providing local charge balance at radiation damage sites.

There has been very little direct evidence for the chemical alteration of zircon in natural systems. The mineral is known to be highly durable in most environments and commonly survives weathering to be recycled in the Earth's crust. However, there are field observations that point to the instability or corrosion of zircon in natural metamorphic or hydrothermal systems with high F concentrations [107,108] and at low temperatures during weathering [109]. Furthermore, Wayne and Sinha [110] have shown that microfractures caused by radiation damage may serve as pathways for aqueous fluids, resulting in preferential leaching of radiation-damaged regions within the zircon grains at temperatures on the order of 450–500°C.

Recent studies at ANSTO have documented the alteration of radiation-damaged, 1000 Ma zircons from a granitic pegmatite in the Grenville Province of Ontario, Canada (G.R. Lumpkin, unpublished data). SEM–EDX analyses show that these zircons contain up to 0.4 wt% ThO_2 and 1.3 wt% UO_2, resulting in alpha-decay doses that completely span the crystalline–amorphous transformation (see Section 4.5). Primary compositional zoning is common in these crystals, consisting of alternating concentric zones characterized by high and low actinide contents. Some of the crystals have a relatively unzoned actinide-rich core surrounded by a heavily fractured rim with the usual concentric zoning, but lower overall actinide concentration. The latter crystals exhibit the most severe alteration. Fig. 9 clearly shows how radiation damage-induced volume expansion of the core caused brittle failure of the rim, resulting in pathways for fluid flow and preferential alteration of the metamict core of the crystal. Relative to the unaltered areas of the core, the altered areas have gained up to 0.6 wt% Al_2O_3, 4.1 wt% CaO, and 0.8 wt% FeO and have lost about 40% of the original amount of U and much of the Th. Interestingly, other analyses of metamict areas of zircon crystals reported in the literature generally have elevated contents of Ca and other elements (e.g., see [111]), suggesting that some chemical alteration has occurred.

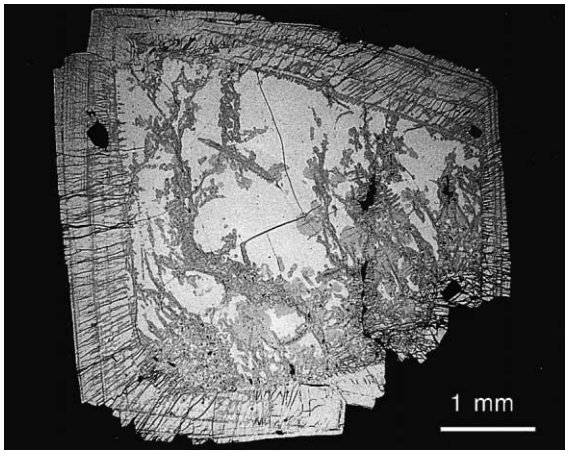

Fig. 9. SEM backscattered electron image of zircon from Ontario, Canada ($t = 1000$ Ma). This is a prime example of the relationship between alpha-decay damage and geochemical alteration. The core of the crystal is U-rich and metamict (1.0–1.3 wt% UO_2). The rim shows concentric bands of alternating crystalline (<0.2 wt% UO_2) zones and partially damaged zones (0.4–0.8 wt% UO_2). Due to the 16–18% volume expansion during amorphization, the rim was heavily fractured and allowed fluids to penetrate to the core, where most of the alteration occurred.

4. Radiation damage effects

4.1. Pyrochlore

The first detailed study of radiation damage in pyrochlore was published by Krivokoneva and Sidorenko [112]. These authors examined 19 pyrochlore samples from Siberian carbonatites using XRD methods, demonstrating that the metamict transformation is a continuous process related to increasing amounts of Th and U in the samples. Pyrochlores with the lowest concentrations of these elements were found to be crystalline with sharp diffraction maxima and well-resolved $K_{\alpha 1,2}$ peaks. With increasing actinide content, $K_{\alpha 1,2}$ peak resolution gradually disappeared, accompanied by line broadening, decreased peak intensities, and the appearance of a weak and very broad maximum. XRD patterns of completely metamict specimens were characterized by two broad 'humps' peaking at approximately 30°2θ and 50–53°2θ. An analysis of the line broadening showed that strain increased from 0.0009 to 0.0035 as crystallite dimensions decreased from 100–120 nm down to 35–40 nm in the initial stages of damage. Further decreases in the crystallite dimensions down to 15 nm were observed in the latter stages of damage prior to complete metamictization. Krivokoneva and Sidorenko [112] also carried out an analysis of the radial distribution function (RDF) of a fully metamict sample and showed that there was no long range order present beyond the second coordination sphere. However, peaks in the RDF representing the major M–O and M–M distances showed that the fundamental structural units (e.g., the coordination polyhedra) still existed in the metamict state.

In their study of microlite from the Harding pegmatite, Lumpkin et al. [45] showed that the samples ranged from highly crystalline to completely amorphous as a function of increasing U content. At about the same time, groups from the University of New Mexico and Los Alamos National Laboratory collaborated on a DTA study of the annealing of natural pyrochlores [113]. The samples investigated had a range of compositions and crystallinity, with alpha-decay doses up to 40×10^{16} α mg^{-1}. Results of this study indicated that the temperature of the exotherm associated with recrystallization varies from 400°C to 700°C, depending upon sample composition and crystallinity (using I/I_0 determined by XRD). Measured values of the recrystallization energy ranged from approximately 125 to 200 J g^{-1} and were inversely correlated with the level of crystallinity. Lower values in the range of 40–125 J g^{-1} were determined for altered pyrochlore samples. In comparison, metamict Nb–Ta–Ti oxide minerals with stoichiometries of ABO_4 and AB_2O_6 also had lower recrystallization energies in the range of 40–85 J g^{-1}.

Subsequently, Lumpkin and Ewing [114] studied 51 pyrochlore samples from 15 different localities ranging in age from 16 to 1400 Ma. The changes in physical properties of these samples were characterized by XRD and TEM as a function of alpha-decay dose. Using the Th and U contents determined by quantitative electron microprobe work, the dose was calculated according to the equation

$$D = 8N_{238}(e^{\lambda_{238}t} - 1) + 6N_{232}(e^{\lambda_{232}t} - 1). \quad (11)$$

In Eq. (11), N_{238} and N_{232} are the present numbers of atoms per mg of U and Th, λ_{232} and λ_{238} are the decay constants of ^{232}Th and ^{238}U, and t is the geologic age. Using XRD to determine both the beginning (D_i) of the crystalline–amorphous transformation as well as the critical amorphization dose (D_c), Lumpkin and Ewing [114] showed that the transformation zone increased in dose as a function of the geological age of the samples. Both dose curves were fitted to an equation of the form

$$D_{i,c} = D_0 e^{tK}. \quad (12)$$

In this expression, D_0 is the intercept dose for D_i or D_c and K is a rate constant. Since Eq. (12) describes the annealing kinetics as a function of time, the value of D_0 provides an estimate of D_i or D_c for very short time periods and high dose rates. These results provided independent support for the annealing of isolated alpha-recoil collision cascades back to the crystalline structure in natural pyrochlore. A more detailed analysis of the dose-age data yielded a value of $D_0 = 1.4 \times 10^{16}$ α mg^{-1} for the amorphization dose curve and $K = 1.7 \times 10^{-9}$ yr^{-1} [115]. Previously, Eyal and co-workers [116–118] showed that long-term annealing rates could be calculated for minerals by using a chemical etching technique combined with measurements of U and Th isotopes in solution. In fully amorphous betafite, the technique indicated that collision cascades anneal or 'relax' to the aperiodic configuration at a rate of approximately 10^{-5}–10^{-6} yr^{-1} [116,119], or about three to four orders of magnitude faster than the annealing of collision cascades back to the crystalline structure.

Lumpkin and Ewing [114] went on to provide a detailed description of the alpha-decay damage process. As shown in Fig. 10, XRD peak intensities decrease in a regular manner with increasing dose, without transformation of the structure to the fluorite subcell, and with no major changes in peak symmetry. After correcting their data for long-term annealing, intensity ratios of the damaged samples were fitted to an equation of the form

$$I/I_0 = e^{-BD}. \quad (13)$$

Here, B is a constant related to the amount of material damaged by each alpha-decay event. The results are shown in Fig. 11. Eq. (13) gave an excellent fit to the data and yielded $B = 2.6 \times 10^{-16}$ mg α^{-1}, corresponding to an average cascade diameter of 4.6 nm in which a

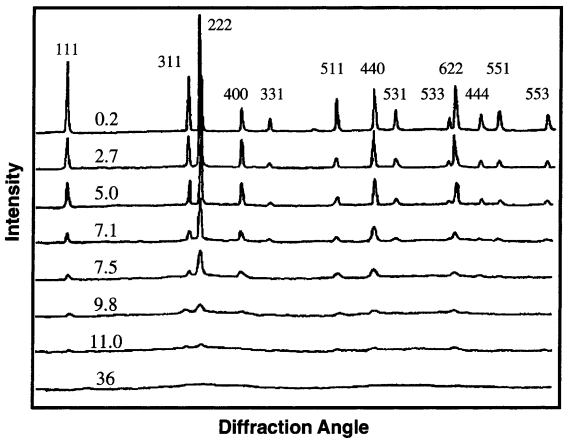

Fig. 10. XRD patterns of Ta-rich pyrochlore (microlite) with variable U content from the Harding pegmatite, New Mexico ($t = 1300$ Ma). The alpha-decay dose is given in units of 10^{16} α mg^{-1}. Note persistence of pyrochlore superlattice peaks (e.g., 111, 311, 331, 511) through the transformation.

maximum of 2600 atoms are displaced. The value of B was shown to be within the range of previous estimates for minerals and synthetic samples doped with ^{238}Pu or ^{244}Cm, lending support to the annealing model. An analysis of line broadening in these samples showed that crystallite dimensions decreased from about 500 to 15 nm as the corrected dose increased from 0.02×10^{16} α mg^{1} to about 1.0×10^{16} α mg^{-1}. Strain increased with dose, reaching a maximum of approximately 0.003, then decreased to values below 0.0005 prior to attainment of the fully amorphous state (see Fig. 11).

The structure of the metamict state in pyrochlore was investigated in 10 fully amorphous samples. An analysis of the diffuse diffraction humps indicated that they were consistent with a range of M–M and M–O distances in the amorphous structure, with no long-range periodicity beyond the second coordination sphere. Average M–M and M–O distances were estimated to be 0.350–0.363 nm and 0.206–0.222 nm, respectively. The results indicated a significant decrease in the M–O distances on the order of 7% relative to the original crystalline structure. During this period, Greegor and co-workers [120–123] carried out several studies of the local structure and bonding around Ti, Nb, Ta, and U atoms in pyrochlore using EXAFS–XANES. Results of these studies demonstrated that the M–O coordination polyhedra of metamict pyrochlore exhibit reduced bond distances, reduced coordination number, and increased distortion relative to the undamaged crystalline structure. Furthermore, there was no periodicity in evidence beyond the second coordination sphere, with some disruption of the M–M distances. From these studies it was realized that only a slight increase in the mean M–M distance was required in order to explain the overall increase in volume caused

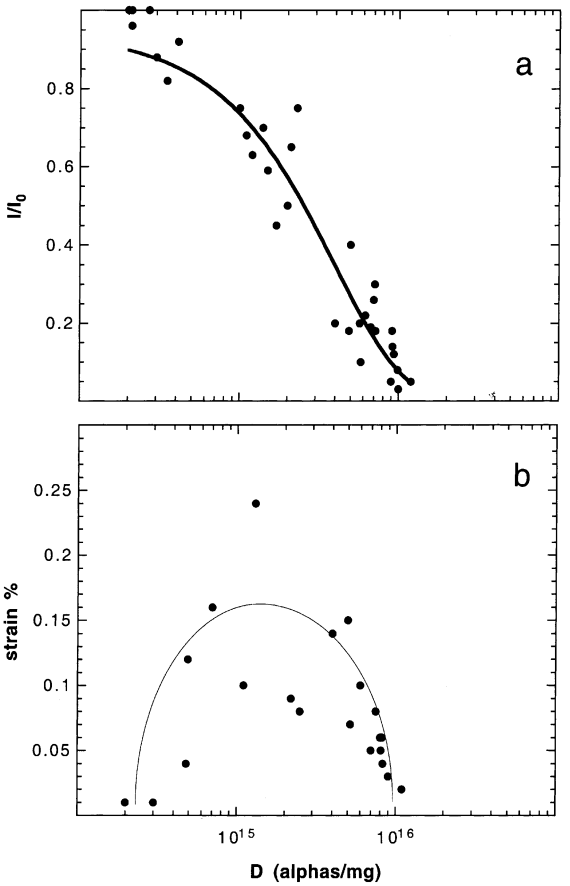

Fig. 11. XRD data for natural pyrochlores after correction of the dose for long-term annealing. (a) Plot of the total diffracted intensity (as I/I_0) versus dose, indicating a critical dose of approximately 1×10^{16} α mg^{-1}. (b) Calculated values of strain derived from measurements of line broadening. Note that strain reaches a maximum part way through the transformation, then decreases.

by alpha-decay damage and that this could be facilitated by increased M–O–M angles.

Changes in the microstructure with increasing dose were investigated by using high resolution TEM [114] (see Fig. 12). Mottled image contrast and local 1–5 nm sized areas of damage provided the first indication of the beginning of the crystalline–amorphous transformation at a corrected dose of about 0.1×10^{16} α mg^{-1}. Local amorphous domains increased in abundance up to 0.2×10^{16} α mg^{-1} and some lattice misorientation (generally less than 5°) was observed in the crystalline areas. At higher corrected dose levels up to 0.7–0.8×10^{16} α mg^{-1}, the crystalline areas diminish in abundance, giving way to a microstructure dominated by amorphous pyrochlore. Lattice fringes were not observed at a corrected dose of 1.2×10^{16} α mg^{-1}, indicating that the amorphous state had been reached.

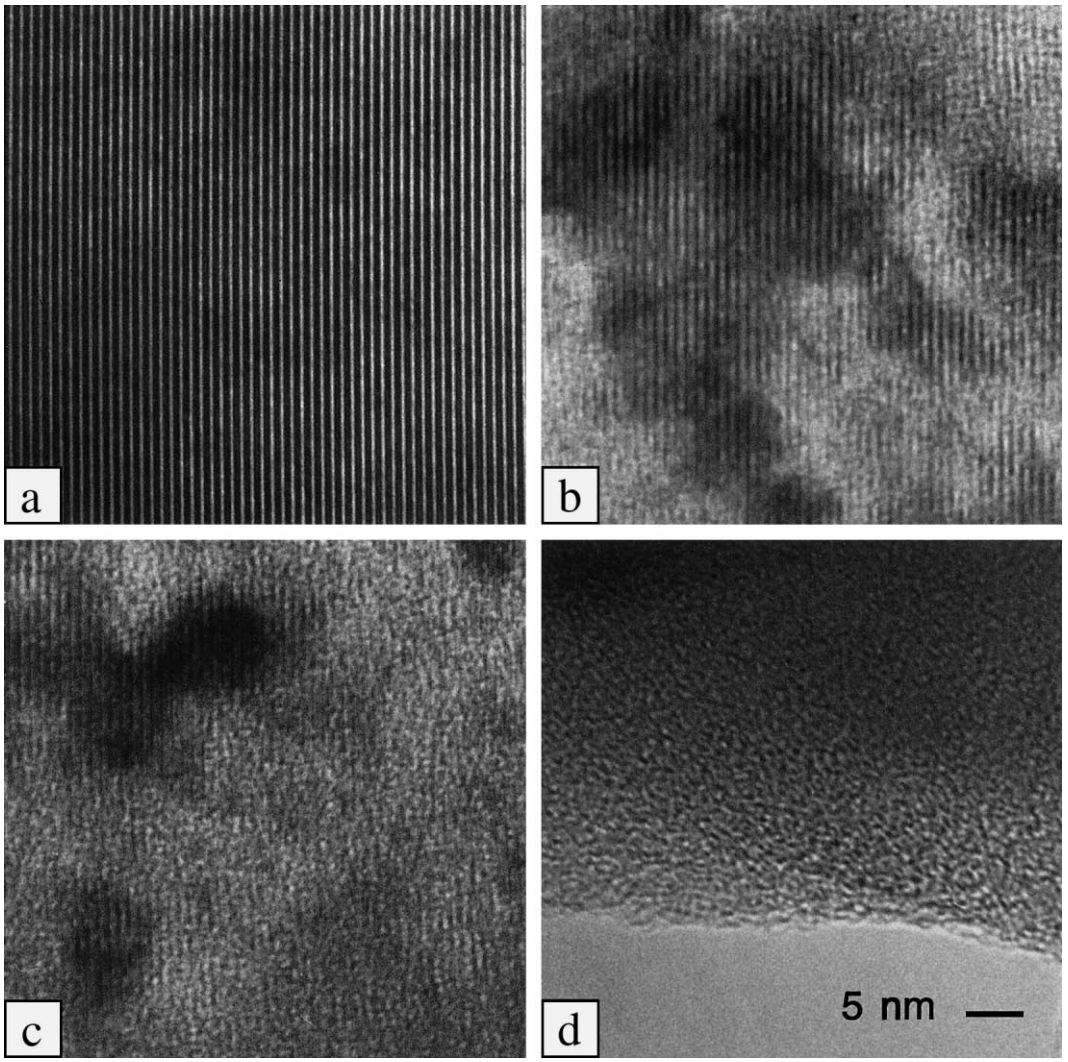

Fig. 12. High resolution TEM images of the crystalline–amorphous transformation in Ta-rich pyrochlore (microlite) from the Harding pegmatite. (a) Highly crystalline sample, $D = 0.2 \times 10^{16}$ α mg^{-1}. (b) Partially damaged sample, $D = 3.5 \times 10^{16}$ α mg^{-1}. (c) Heavily damaged sample, $D = 9.6 \times 10^{16}$ α mg^{-1}. (d) Completely amorphous sample, $D = 13.8 \times 10^{16}$ α mg^{-1}.

Electron diffraction patterns were initially recorded for [110] zone axis conditions and then [111] systematic row conditions through most of the transformation (Fig. 13). The patterns revealed gradually diminishing Bragg spots and increasing diffuse rings with equivalent d-spacings of 0.30 and 0.18 nm. There was no definitive evidence for conversion to the fluorite subcell as the (1 1 1) diffracted beams and other superlattice spots were observed throughout the transformation.

4.2. Zirconolite

Sinclair and Ringwood [31] published the initial work on radiation damage in zirconolite in 1981 using XRD and TEM. Results of this study indicated that zirconolites retain substantial crystallinity up to a doses of 2×10^{16} α mg^{-1} and higher. These conclusions were mainly based on the TEM observation of polycrystalline material in a sample from Sri Lanka. Electron diffraction patterns of these areas gave sharp, spotty ring patterns consistent with the structure of fluorite. Other areas of the Sri Lanka zirconolite sample had low contrast and only showed diffuse rings in the diffraction pattern, which the authors went on to interpret as also being representative of the principal lattice spacings of the fluorite structure type. Subsequently, Ewing and Headley [124] examined similar zirconolite specimens by TEM and concluded that those at the highest dose levels

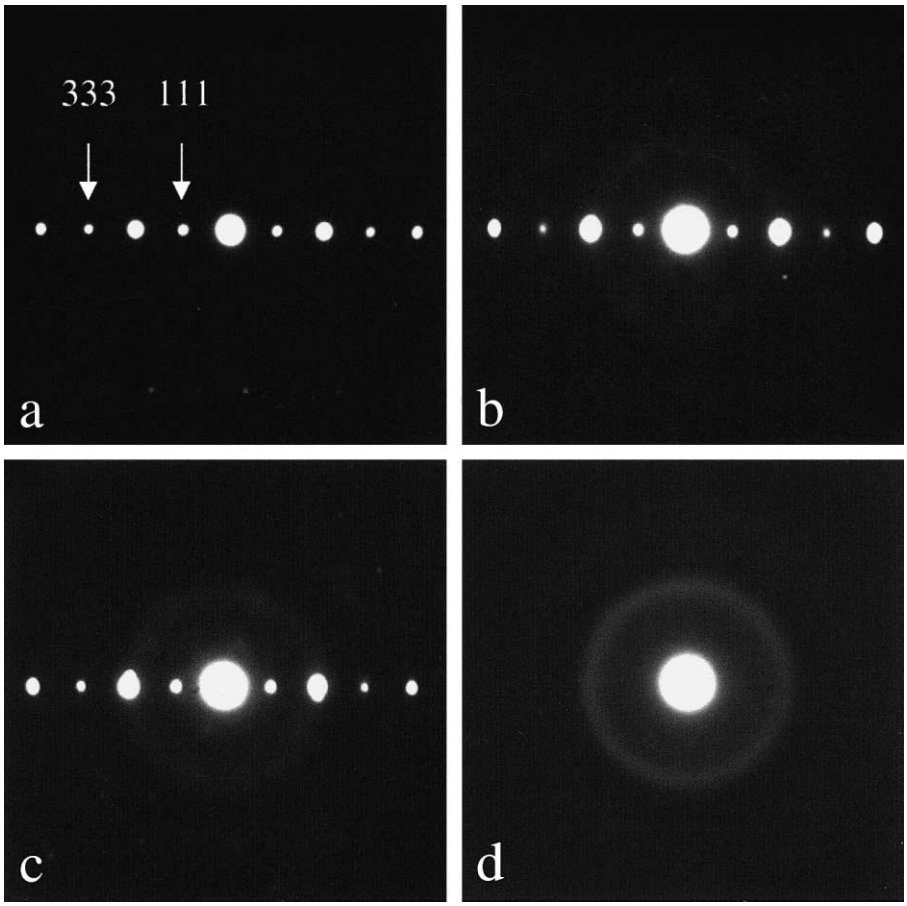

Fig. 13. Selected area electron diffraction patterns of the crystalline–amorphous transformation in Ta-rich pyrochlore (microlite) from the Harding pegmatite. Note the persistence of the (1 1 1) superlattice spots through the transformation. Patterns shown in (a)–(d) correspond to the images shown in Fig. 12(a)–(d).

were in fact electron diffraction amorphous with an inner diffuse ring spacing of 0.304 nm. Furthermore, they demonstrated that the polycrystalline microstructure observed by Sinclair and Ringwood was caused by electron beam heating. In the discussion of their findings, Ewing and Headley noted that the d-spacing of the inner diffuse ring of metamict zirconolite is similar to that of many other metamict oxide and silicate minerals. The authors concluded that the structure of metamict zirconolite was non-periodic at the image resolution of their TEM (1.0–1.5 nm for discreet crystalline domains).

Following these investigations, additional work was carried out on metamict and annealed zirconolite from Sri Lanka using a variety of methods, including XRD, EXAFS–XANES, TEM, and DTA [125,126]. Electron diffraction and high resolution TEM studies suggested that metamict zirconolite lacked periodicity beyond the second coordination sphere, consistent with a random network model of the amorphous state. EXAFS–XANES results provided more detailed information for the Ti- and Ca-sites and indicated that metamict zirconolite lacked periodicity beyond the first coordination sphere, with reduced M–O bond lengths, reduced coordination number, and increased distortion of the Ti–O polyhedra (determined from a prominent pre-edge feature in the XANES results). Farges et al. [127] provided additional results for the Zr-, Th-, and U-sites and reported nearly identical coordination numbers and bond lengths for the metamict and annealed samples. However, a significant increase in the range of Zr–O and Th–O distances was observed, leading the authors to conclude that slight variation of the M–O–M angles can have a profound effect on long-range periodicity and medium-range order. Later work also confirmed the reduced coordination of Ti in the metamict samples, pointing specifically to a five-fold coordination geometry [128].

Annealing studies of the metamict zirconolites from Sri Lanka were performed using DTA and showed exotherms at approximately 780°C due to recrystalliza-

tion [125]. For two different samples, the energy release associated with recrystallization was 43 and 48 J g^{-1}. TEM investigation of samples annealed at 1100°C showed that the structure recovered to monoclinic zirconolite-2 M, but the material was highly twinned and contained some stacking faults and intergrowths of other polytypes on (0 0 1). A few polycrystalline grains were also observed which gave electron diffraction patterns consistent with the fluorite structure type. From these observations, Lumpkin et al. [125] suggested that metamict zirconolite initially recrystallizes to a disordered, defect fluorite structure.

In spite of advances in the understanding of alpha-decay damage in natural zirconolite, a detailed characterization of the crystalline–amorphous transformation remained elusive until 1994, when Lumpkin and colleagues [129,130] developed and tested procedures for accurate microanalysis of zirconolite for up to 25 elements using AEM thin-film methods. Using these procedures, it was shown that very small volumes of a given sample could be characterized by electron diffraction and imaging and the measured concentrations of Th and U could be used to calculate the dose from Eq. (11). A detailed study of highly zoned samples from Bergell (Switzerland) and Adamello (Italy) provided the first detailed results on the crystalline–amorphous transformation in natural zirconolites [130]. Fig. 14 shows the characteristic grain size and complex zoning patterns of samples from Bergell. Note that in some crystals, the chemical zones may be dimensionally below the resolution of the electron probe in EPMA or SEM–EDX instruments. The ThO_2 and UO_2 concentrations obtained by AEM on crystals from both localities are plotted in Fig. 15 and contoured for dose, demonstrating the substantial range of alpha-decay dose in these samples. In particular, a series of dark field images (see Fig. 16) present a dramatic illustration of the changes in microstructure with increasing dose. These images illustrate the appearance of mottled diffraction contrast (0.08×10^{16} α mg^{-1}), extensive development of amorphous domains in a crystalline matrix ($0.3–0.5 \times 10^{16}$ α mg^{-1}), and overlap of collision cascades to produce larger amorphous areas with crystalline domains reduced in size to less than 10 nm ($0.7–0.9 \times 10^{16}$ α mg^{-1}).

Preliminary results were recently presented for seven suites of zirconolite samples ranging in age from 16 to

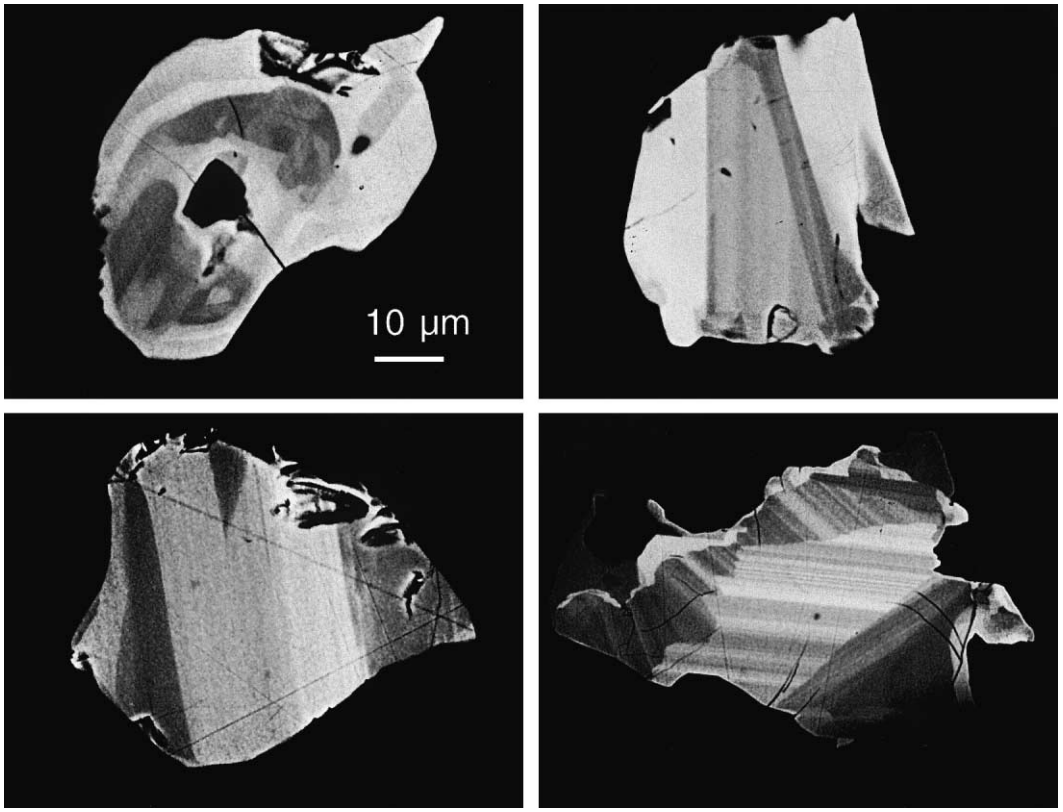

Fig. 14. Backscattered electron images of zoned zirconolite crystals from Bergell, Switzerland ($t = 31$ Ma). Compositional zoning is primarily due to variations in the REE and ACT contents. Note that very few microcracks are present in these grains (see Fig. 15 for dose variation).

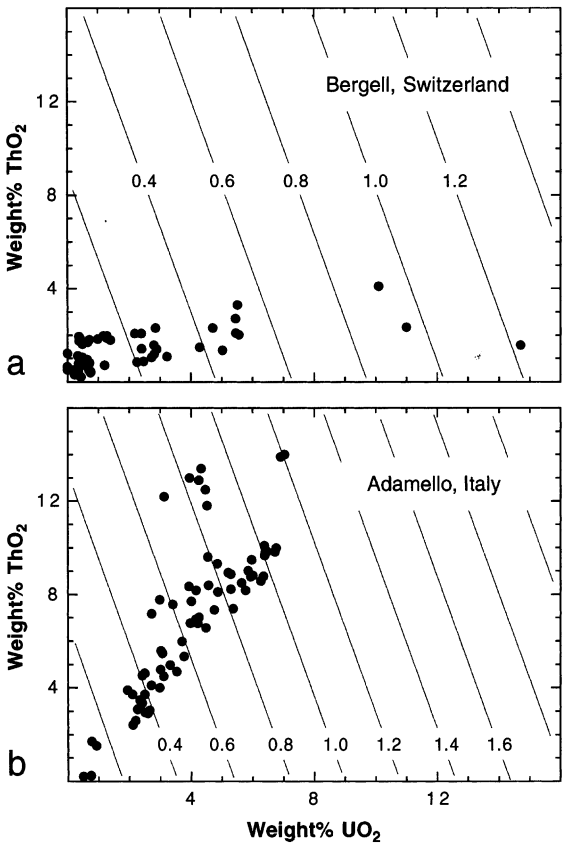

Fig. 15. Plots of ThO_2 versus UO_2 for zoned zirconolites from Bergell, Switzerland and Adamello, Italy. The figures are contoured for alpha-decay dose in units of 10^{16} α mg^{-1} using geological ages of 31 Ma and 42 Ma, respectively. These data were determined entirely by AEM and demonstrate that both suites of zirconolite samples completely span the crystalline–amorphous transformation.

2060 Ma and in dose from 0.008×10^{16} to 24×10^{16} α mg^{-1} [131]. For each suite of samples, the beginning of the crystalline–amorphous transformation (onset dose) was defined as the first appearance of mottled diffraction contrast in bright field images. The end of the transformation (critical amorphization dose) was defined by the complete disappearance of Bragg diffraction spots, leaving only diffuse rings at approximately 3.0 and 1.8 Å in diffraction patterns. These dose 'brackets' were used to construct a plot of dose versus age, revealing a pattern of upward curvature with increasing age for both the onset dose and critical dose. As in the previous work on pyrochlore, this upward curvature was interpreted as evidence for long-term annealing of isolated alpha-recoil collision cascades back to the crystalline structure. The data were fitted using Eq. (12) in order to determine the intercept dose and annealing rate constant. Curve fits gave values of $D_0 = 0.11 \times 10^{16}$ α mg^{-1} and $K = 1.0 \times 10^{-9}$ yr^{-1} for the onset dose curve; and $D_0 = 0.94 \times 10^{16}$ α mg^{-1} and $K = 0.98 \times 10^{-9}$ yr^{-1} for the critical dose curve.

Lumpkin et al. [131] also presented the first information bearing on the thermal histories of the natural zirconolite samples. In the case of the Bergell intrusion, the thermal history is well constrained by thermochronology, a method of time–temperature path analysis that relies on age dating techniques with different closure temperatures (e.g., U–Th–Pb, K–Ar, Rb–Sr, and fission track dating). Fig. 17 presents the cooling history of the Bergell intrusion, showing that the rocks cooled rapidly from approximately 600°C to 300°C in the first 3–4 Ma, then cooled much more slowly to 100°C in the next 15 Ma. From these data, an average effective temperature of 185°C was calculated for the intrusion. Using a simple model of conductive heat flow together with the available geological information, estimates of the average effective temperature were derived for four other zirconolite localities. The combined data indicate that the zirconolites have been stored in the earth's crust at average temperatures of 100–200°C.

4.3. Perovskite

At present, very limited amounts of data are currently available for alpha-decay damage in natural perovskites. Sinclair and Ringwood [31] examined perovskite samples having doses up to 0.3×10^{16} α mg^{-1} and reported that the XRD patterns gave no significant evidence of radiation damage. From this limited data set they suggested that perovskite is more resistant to the effects of radiation damage than zirconolite. A review of the literature by Van Konynenburg and Guinan [132] indicated that the beginning of the crystalline–amorphous transformation (using a 1% swelling criterion) was reached after a dose of approximately 0.1×10^{16} α mg^{-1}, similar to zirconolite. The X-ray amorphous condition could not be accurately constrained, but appeared to be between 0.3 and 3×10^{16} α mg^{-1} from the available data.

The problem of radiation damage in natural perovskite was recently revisited by Lumpkin et al. [133] using the AEM techniques described in Section 4.2 and a large suite of samples having a range of geological ages. Unfortunately, due to the low Th and U contents (0.1–0.8 wt% ThO_2, <0.2 wt% UO_2), most of the samples were found to be highly crystalline. Dose-age data for three suites of samples bracket the beginning of the crystalline–amorphous transformation based on the first appearance of mottled diffraction contrast in TEM images. Perovskite grains containing 1.4–3.1 wt% ThO_2 indicate that the beginning of the transformation is at a dose of $0.3–0.6 \times 10^{16}$ α mg^{-1} for $t = 295–520$ Ma. A preliminary analysis of the data using Eq. (12) gave $D_0 = 0.19 \times 10^{16}$ α mg^{-1} and $K = 2.3 \times 10^{-9}$ yr^{-1}. The

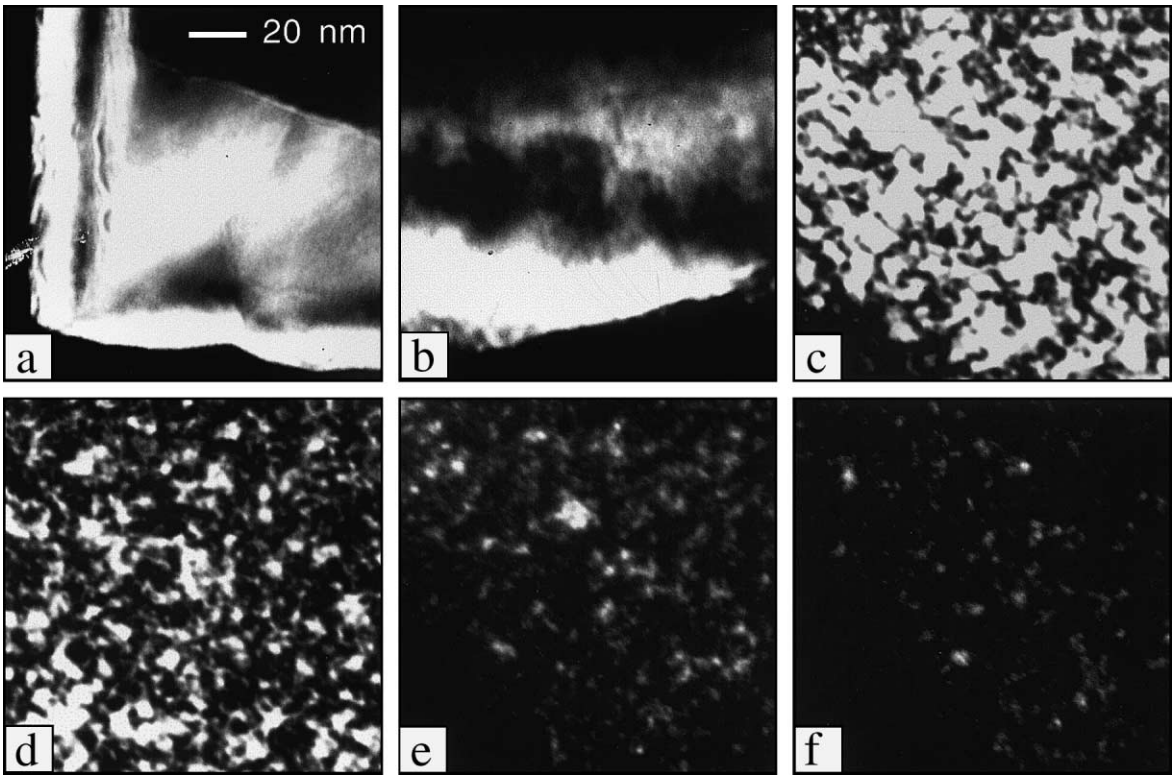

Fig. 16. TEM dark field images of zirconolites from Bergell, Switzerland and Adamello, Italy showing alpha-decay damage microstructures as a function of increasing dose. (a) Undamaged zirconolite, $D = 0.03 \times 10^{16}$ α mg^{-1}. (b) Slightly damaged, $D = 0.08 \times 10^{16}$ α mg^{1}. (c) Moderately damaged, $D = 0.3 \times 10^{16}$ α mg^{-1}. (d) Moderately damaged, $D = 0.5 \times 10^{16}$ α mg^{-1}. (e) Heavily damaged, $D = 0.7 \times 10^{16}$ α mg^{-1}. (f) Heavily damaged, $D = 0.9 \times 10^{16}$ α mg^{-1}.

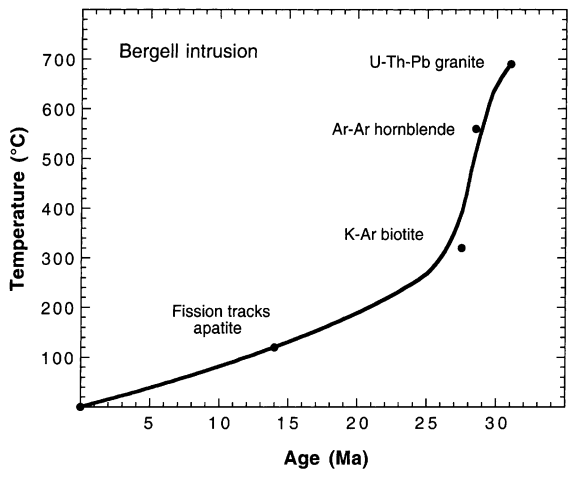

Fig. 17. Thermal history of the Bergell intrusion deduced from U–Th–Pb dating of the granite, Ar–Ar dating of hornblende, K–Ar dating of biotite, and fission track dating of apatite. Note the very rapid cooling to about 300°C, followed by a much longer period of slow cooling.

results presented here suggest that natural perovskite may be more 'resistant' to radiation damage than zirconolite. Lumpkin et al. [133] suggested that this result is probably not due to differences in thermal history, as zirconolite and perovskite occur at many of the same localities used to produce the dose-age plots. Thus it appears that there may be an intrinsic difference between the two minerals.

A few perovskite grains from Bratthagen contain up to 6.0 wt% ThO_2 and have calculated alpha-decay doses of $0.8–1.2 \times 10^{16}$ α mg^{-1}. These grains appear to be moderately damaged based on the appearance of a weak diffuse ring in electron diffraction patterns (see Fig. 18). In comparison, the observed dose of the altered perovskite described in Section 3.3 is approximately $1.5–1.7 \times 10^{16}$ α mg^{-1} and this material is completely electron diffraction amorphous as shown in Fig. 18. Two possible scenarios could explain the lower amorphization dose of altered loparite from Bratthagen. In the first scenario, alteration occurred before the accumulation of significant radiation damage, implying that the altered loparite is less resistant to alpha-decay damage. The second possibility involved late alteration after amor-

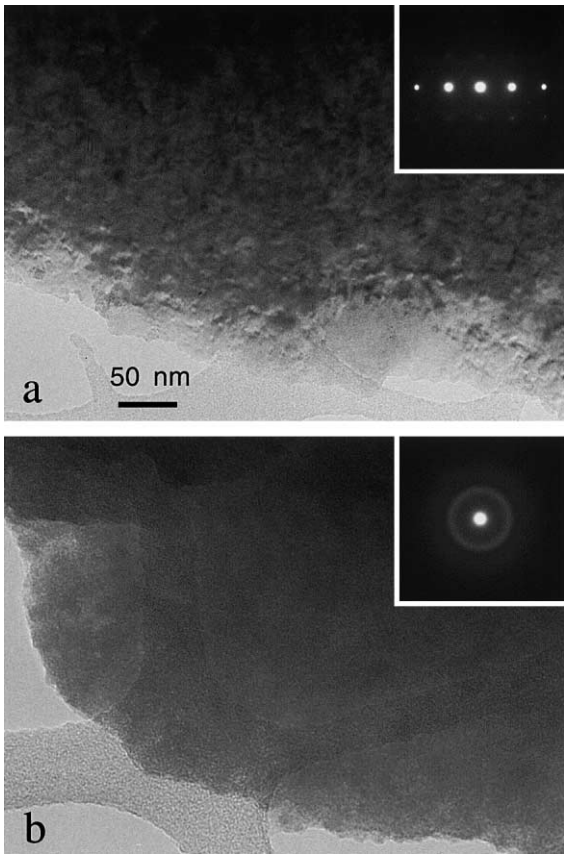

Fig. 18. TEM images and electron diffraction patterns of perovskite (loparite) from Bratthagen, Norway. (a) Microstructure of partially damaged loparite showing the classic mottled diffraction contrast. (b) Microstructure of the fully amorphous, metaloparite alteration product (see SEM images in Fig. 6).

phization of perovskite, possibly implying a radiation damage enhanced susceptibility to alteration. If significant loss of Th occurred during alteration, this would lead to an underestimate of the dose based on the present day Th content [133].

Loparite and altered loparite samples from the Burpala alkaline complex, Russia, have been studied by Chakhmouradian et al. [93] using EPMA and XRD. Loparite samples were found to contain 2.1–5.2 wt% ThO_2 and up to 0.3 wt% UO_2 and were determined to be pseudocubic with very weak orthorhombic diffraction peaks; whereas, the altered loparite samples contained 1.8–6.0 wt% ThO_2 and up to 0.5 wt% UO_2 and were XRD amorphous. Using Eq. (11) and an age of 500 Ma from Oversby and Ringwood [32], dose ranges of $0.6–2.0 \times 10^{16}$ and $0.5–4.0 \times 10^{16}$ α mg^{-1} are obtained for loparite and altered loparite, respectively. These data are entirely consistent with the general dose-age data presented by Lumpkin et al. [133] and, because the alteration of perovskite occurred relatively early in the Burpala complex, they tend to support the first scenario discussed in the preceding paragraph.

Th-rich loparite samples from the Khibina alkaline complex, Russia, have also been studied by EPMA and XRD [89]. The crystals are zoned and contain 2.3–18.5 wt% ThO_2, increasing from core to rim. XRD results indicate that the cores (2.3–7.4 wt% ThO_2) retain some crystallinity, but the rims (8.7–18.5 wt% ThO_2) are completely metamict. The authors did not report dose data, but using Eq. (11) and an age of 380 Ma [32], maximum doses of 1.7×10^{16} and 4.2×10^{16} α mg^{-1} are obtained for the cores and rims, respectively. These results suggest that the critical dose of the Khibina loparite is just below the 'expected position' estimated by Lumpkin et al. [133].

4.4. Brannerite

Previous XRD work has indicated that brannerite is usually metamict in nature [102,103], but no systematic studies were made until recently when Lumpkin et al. [101] examined a small group of samples ranging in age from approximately 25 Ma up to 1580 Ma using SEM–EDX and TEM methods. The available TEM results are summarized in Fig. 19 using a relatively young sample from Switzerland. Electron diffraction patterns of relatively unaltered areas of the brannerite samples typically consist of two broad, diffuse rings characteristic of amorphous materials. The diffuse rings have equivalent d-spacings of 3.1 and 1.9 Å, similar to many other metamict oxides and certain silicate minerals [124]. Bright field images of these grains are typically featureless, consistent with the absence of long-range periodicity. None of the samples examined by TEM showed the presence of significant crystalline domains of brannerite. In samples where crystallinity is observed, it is usually minor and can be attributed to inclusions of uraninite or other trace minerals, precipitates of galena resulting from Pb migration, or secondary phases associated with alteration (e.g., anatase).

Based on the Th and U contents and either the known age or the chemical U–Pb age determined by SEM–EDX, the brannerites have average alpha-decay doses of $2–170 \times 10^{16}$ α mg^{-1}. Unfortunately, the critical amorphization dose cannot be determined from these samples because none of the grains have retained crystallinity. However, using literature data for a partially crystalline brannerite from Binntal, Switzerland [134], the critical dose appears to be close to $1–3 \times 10^{16}$ α mg^{-1} for an age of 10–20 Ma. This result is only slightly higher than the critical dose curves of natural pyrochlore and zirconolite for this range of geological age [114,115,131]. The available data indicate that brannerite samples with ages of approximately 1–10 Ma are required to characterize the crystalline–amorphous transformation.

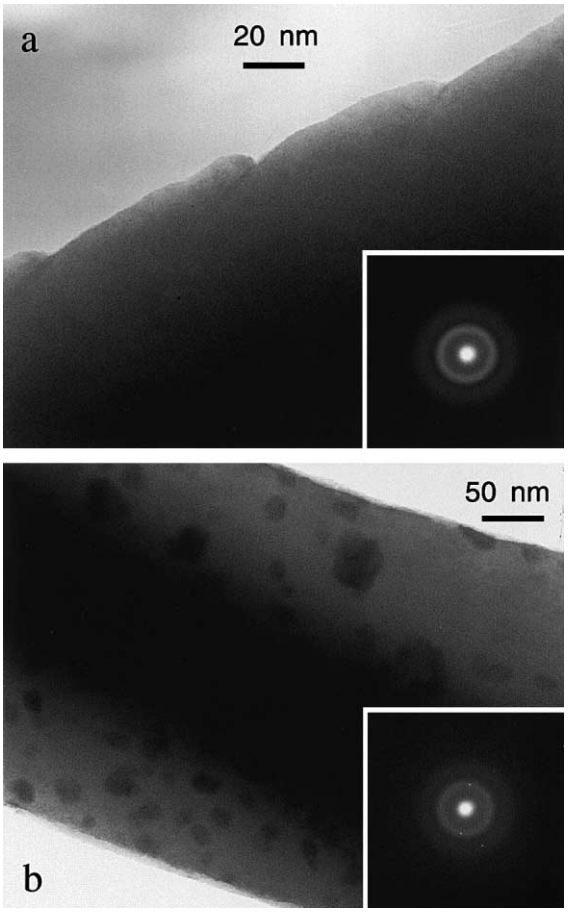

Fig. 19. TEM images and electron diffraction patterns of fully amorphous brannerite. (a) Sample from Ticino, Switzerland. Note the complete absence of diffraction contrast in the image. Selected area diffraction pattern only shows diffuse rings with equivalent d-spacings of about 0.30 and 0.19 nm. (b) Sample from Cordoba, Spain. Bright field image shows inclusions of crystalline UO_2 in amorphous brannerite. Diffraction pattern shows diffuse rings from the brannerite and weak Bragg spots from the inclusions.

4.5. Zircon

In their study of natural zircons from several different localities, Hurley and Fairbairn [23] demonstrated that the mineral experiences a transformation from the crystalline to the metamict state over a finite dose range using XRD. Using information on the geological age and measured alpha activity to calculate the dose, they determined that the diffraction angle of the (1 1 2) reflection decreased from 35.635°2θ to 35.1°2θ with increasing dose up to approximately 0.4×10^{16} α mg^{-1}. The data were found to follow an exponential function that related the 'fractional disorder' to the alpha activity, the number of atoms displaced per alpha-decay, and an annealing parameter. From the data, Hurley and Fairbairn determined a value of $B = 2.3 \times 10^{-16}$ mg α^{-1} and calculated that 4500 atoms were displaced by each alpha-decay event. Their data for zircon samples of different age also suggested that the annealing rate was not significant relative to the dose rate.

The classic study by Holland and Gottfried [24] was carried out on a suite of zircon crystals obtained from the gem gravel deposits of Sri Lanka. Holland and Gottfried studied the density, refractive indices, and unit cell parameters as a function of dose which they also calculated from the age and measured activity of the samples. The density decreased systematically from less than 4.7 g cm^{-3} to approximately 3.96 g cm^{-3} at a dose above 1.2×10^{16} α mg^{-1}. These data showed that the density of zircon decreased by 16% during the process of amorphization. Refractive indices also decreased systematically and approached a single isotropic value of 1.81 over a similar dose range defined by the density measurements. XRD work revealed that the a and c cell parameters both increased rapidly, but anisotropically, as a function of dose before levelling off at approximately 0.6×10^{16} α mg^{-1}. Holland and Gottfried concluded their paper with an analysis of the fractions of crystalline zircon, an intermediate phase (identified by XRD), and amorphous zircon as a function of dose. Importantly, a kinetic analysis of the data showed that $B = 3.8 \times 10^{-16}$ mg α^{-1} based on the decrease in the crystalline fraction as a function of dose. Later work by Lipova et al. [135] generally confirmed the results presented above, but also indicated that some crystallinity is maintained in 1800 Ma zircon up to doses of $9–14 \times 10^{16}$ α mg^{-1}. This was perhaps the first indication of an effect of long-term annealing on the critical amorphization dose of zircon and was later confirmed by Lumpkin and Ewing [114] using literature data for zircon samples from different localities and having a range of geological ages.

Detailed XRD studies of zircons from Sri Lanka have also been carried out by Murakami et al. [136,137]. In this work, the authors followed the profile of the (2 0 0) reflection and made the important observation that the peak could be deconvoluted into a Bragg component and a diffuse scattering component (caused by interstitial defects [138]) with increasing dose. Refinement of lattice parameters before and after removal of the diffuse scattering component showed that the true lattice parameters (Bragg peak only) were somewhat larger at the higher dose values. This procedure enabled a more accurate determination of the anisotropic expansion with increasing dose, giving a lattice volume expansion of 4.7% [136]. Further work, including density measurements and TEM observations, delineated three stages of damage in the natural zircon samples. In stage I ($<0.3 \times 10^{16}$ α mg^{-1}) the damage is dominated by accumulation of point defects, unit cell expansion,

and lattice distortion. Stage II (0.3–0.8 $\times 10^{16}$ α mg^{-1}) is characterized by the overlap of alpha-recoil tracks to produce progressively larger amorphous domains with increasing dose. Finally, in stage III (>0.8 $\times 10^{16}$ α mg^{-1}) the zircon is completely X-ray and electron diffraction amorphous [137].

Earlier results indicated that the metamict state was characterized by misoriented crystallites approximately 10 nm in size [139] or by the presence of precipitates of ZrO_2 [140]. However, the TEM results of Murakami, Headley, and others [137,141] indicate that ZrO_2 and SiO_2 do not occur as the final products of amorphization, at least at relatively low temperatures. Recent studies using Raman spectroscopy [142] are in agreement with this contention. Although some evidence has been documented in the TEM studies for the presence of misoriented domains *during* the transformation, the final state of damage appears to be truly aperiodic. In this connection, Ellsworth et al. [143] have presented data on the energetics of radiation damage in natural zircon as a function of dose using transposed temperature drop calorimetry. Their results showed a large enthalpy of annealing plateau of −59 kJ mol, suggesting that 'the damage to the structure is pervasive on the scale of Ångstroms, consistent with the loss of mid-range order characteristic of a glass'. Nevertheless, the authors note that the energetics do not preclude some chemical heterogeneity due to segregation of Zr and Si.

Changes in the mechanical properties of zircon as a function of dose are extremely important. This is not surprising in view of the large total volume expansion and anisotropic unit cell expansion documented above. Chakoumakos et al. [144] provided a dramatic illustration of the fracture properties of a zoned zircon sample from Sri Lanka. Even though the total $ThO_2 + UO_2$ concentration only varied by about 0.4–0.5 wt% between the 5–400 μm thick growth zones, the variation in dose was sufficient to cause microfracturing of the more brittle, low dose zones. The fractures were pinned in the high dose zones, indicating an increase in fracture toughness for these actinide-enriched layers. Following this work, Chakoumakos et al. [145] revisited the sample and examined in detail the changes in chemistry and mechanical properties using EPMA data and a mechanical properties microprobe (MPM). Results of this study demonstrated that the hardness and elastic modulus of natural zircon decreased by 40% and 25%, respectively, for alpha-decay doses ranging from 0.3 to 1.0 $\times 10^{16}$ α mg^{-1}. An example of the compositional zoning and microfracturing is presented in Fig. 20.

Murakami et al. [137] and Weber and co-workers [146–148] made a significant contribution toward the understanding of alpha-decay damage and annealing in zircon through a comparison of natural samples and synthetic specimens doped with short-lived ^{238}Pu. These comparative studies have demonstrated that differences in dose rate had no major effect on the radiation damage process and that the natural samples experienced significant annealing of point defects and isolated damage tracks over geological time scales at ambient temperatures. Furthermore, annealing of defects resulted in a 'delay' in the onset of amorphization to dose values of approximately 0.09–0.10 $\times 10^{16}$ α mg^{-1}. The authors also determined that a double overlap model best explains the accumulation of amorphous domains, with values of $B = 3.3$–5.9×10^{-16} mg α^{-1} depending on the data set used in the analysis. However, until recently, the fraction of amorphous material as a function of dose has never been measured. Using XRD, Ríos et al. [149] directly measured the amorphous fraction in a suite of zircon samples from Sri Lanka, covering a dose range from 0.006 $\times 10^{16}$ to 1.6 $\times 10^{16}$ α mg^{-1}. The dose dependence of the amorphous fraction (f_a) is shown to follow a direct impact model of amorphization

$$f_a = 1 - e^{-BD}. \tag{14}$$

Note that this expression is related to Eq. (13) if one assumes that I/I_0 is a measure of the crystalline fraction (f_c) and that $f_a + f_c = 1$. The best-fit of Eq. (14) to the data gives a value of $B = 2.7 \times 10^{-16}$ mg α^{-1}, consistent with amorphous cascades having diameters of ~5 nm. These data are remarkably similar to the XRD results described in Section 4.1 for pyrochlore using Eq. (13).

Weber et al. [150] have also suggested a long-term annealing rate of approximately 1 $\times 10^{-9}$ yr^{-1} for zircon from Sri Lanka, a value that is similar to that reported for natural zirconolite [131]. The critical amorphization dose has also been modeled as a function of time and temperature using kinetic data derived from ion beam irradiation experiments on thin film samples [151], performed in the HVEM Tandem Facility at Argonne National Laboratory. Calculations for zircon suggest that the natural samples have been held at effective temperatures on the order of 100–115°C [151]. More recently, Meldrum et al. [152,153] have provided a general expression relating the present day concentration of equivalent U (N_c) for amorphization of zircon as a function of time (t) and temperature (T):

$$N_c = \left[\frac{6 \times 10^6 \times D_0}{[1 - e^{E_a/kT_c(1-T_c/T)}](e^{\lambda t} - 1)nx}\right]. \tag{15}$$

In this expression, D_0 (in units of dpa) is the critical dose at zero Kelvin and E_a is the activation energy for irradiation-enhanced annealing of damage, both of which are determined experimentally from ion irradiation of thin film samples. T_c is the critical temperature above which amorphization does not occur, k the Boltzmann's constant, n the average number of atomic displacements per alpha-decay, x the number of alpha-decays in the decay chain, and λ is the decay constant of ^{238}U. Using Eq. (15), Meldrum et al. [152,153] have

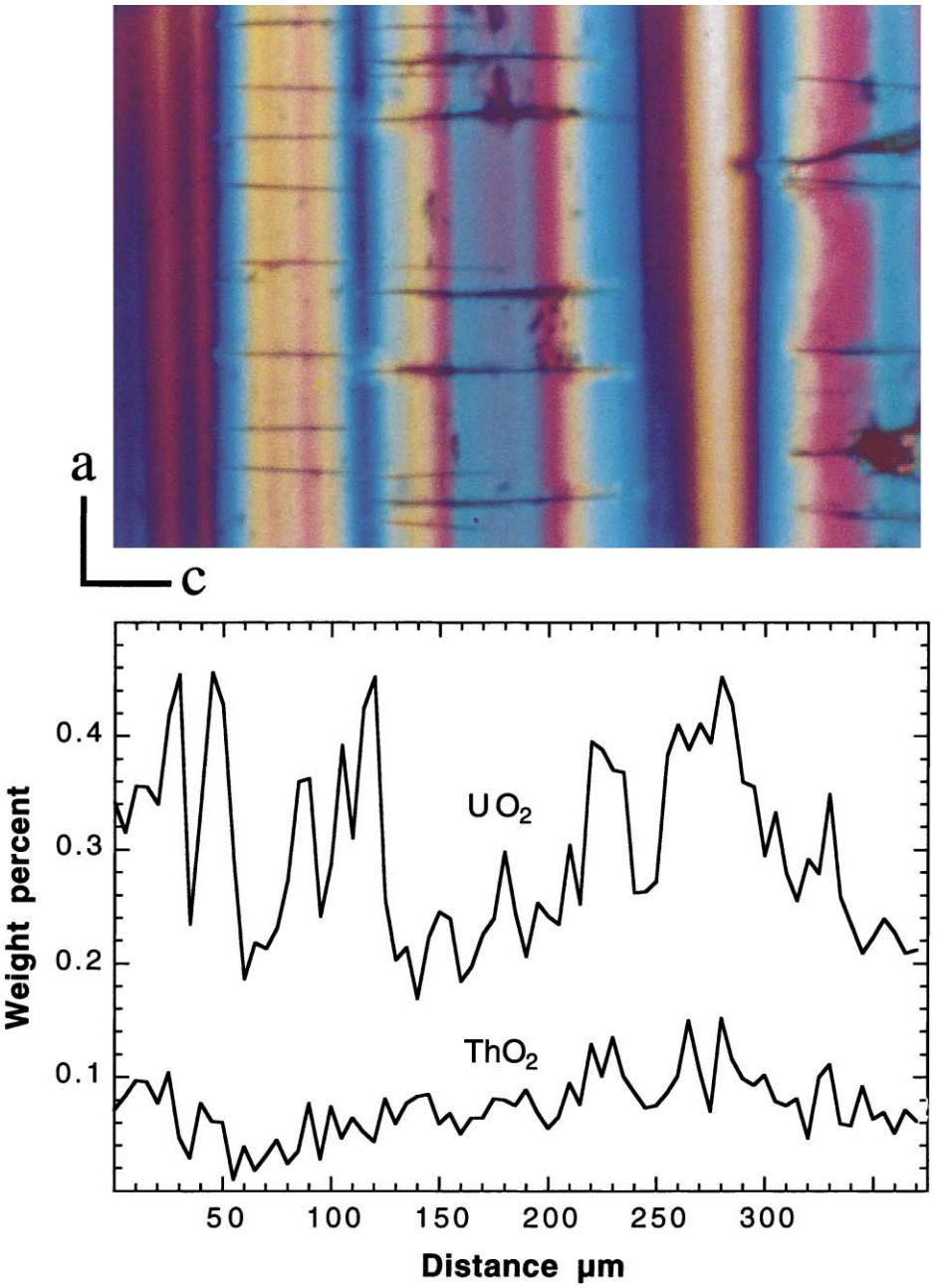

Fig. 20. Optical micrograph and concentration profiles for UO_2 and ThO_2 in zoned zircon from Sri Lanka ($t = 570$ Ma). Note the small range of UO_2 concentration between zones and the severe microcracking resulting from the 16–18% volume expansion caused by alpha-decay damage. The cracks are tensional in nature and are confined to the crystalline zones, a direct result of the stress field induced by the heavily damaged zones. The crystal is viewed down [0 1 0] and the compositional zones are parallel to (0 0 1).

shown that a temperature of about 100°C gives a reasonable fit to the available data for natural zircons ranging in age from less than 100 Ma to 4.2 Ga. Potential problems with this approach include the initial assumptions involved in the derivation of Eq. (15) and the fact that zircon exhibits two-stage annealing behavior during ion irradiation [153]. Furthermore, Eq. (15) does not explicitly account for long-term annealing and this has been modelled separately by calculating the effect of annealing on T_c over geological time periods [152,153]. Finally, the thermal histories of the zircon samples are generally unknown and need to be

determined in order to provide confirmation of the model temperatures.

Recently, the Materials Characterisation Group at ANSTO have obtained new AEM data on the critical dose of 1000 Ma zircon samples from Ontario, Canada. Using unaltered areas of zoned crystals similar the one shown in Fig. 9, we have found that the zircons become metamict at U concentrations between 1.1 wt% and 1.3 wt% UO_2, providing a bracket of D_c at a value of 3.6×10^{16} α mg^{-1}. AEM results also demonstrate that regions of the crystals with lower U contents are partially damaged, but a bracket for the beginning of the transformation is not yet available for these samples. Examples of the microstructure and diffraction patterns of these zircon specimens are shown in Fig. 21. Although we are in the process of refining the dose-age data for zircon (and pyrochlore), the available data for the critical dose have been examined using Eq. (12), giving $D_0 = 0.4 \times 10^{16}$ α mg^{-1} for the critical amorphization dose and $K = 2.1 \times 10^{-9}$ yr^{-1}.

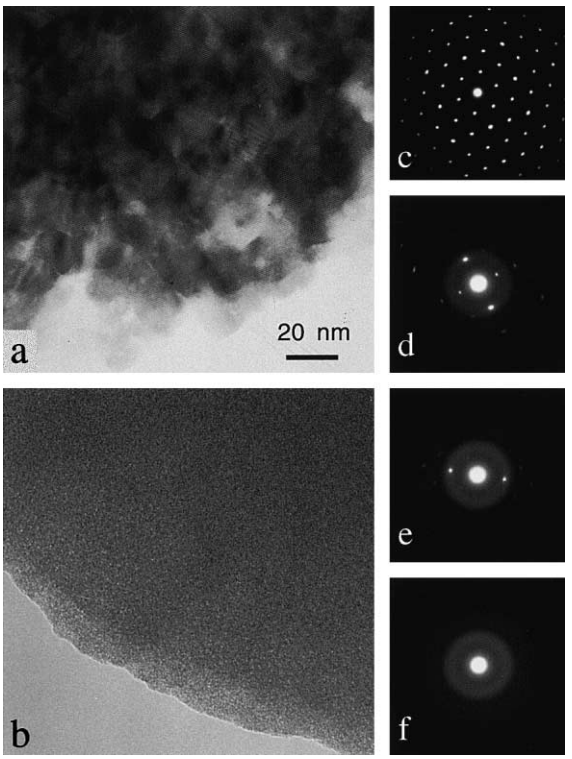

Fig. 21. TEM images and selected area electron diffraction patterns showing radiation damage in unaltered areas (e.g., low Ca content) of zoned zircon from Ontario, Canada (see Fig. 9). A complete characterization of the crystalline–amorphous transformation is available from these 1000 Ma samples due to the range of U and Th contents in the different zones. (a) Image of a slightly damaged grain showing mottled diffraction contrast. (b) Image of a completely amorphous grain. (c)–(f) Typical diffraction patterns with increasing dose from top to bottom.

5. Discussion

5.1. Aqueous durability

The data summarized in this paper allow us to establish a relative ranking of the durability of several actinide host phases in natural systems. In terms of total matrix dissolution, especially at low temperatures, studies of natural samples indicate that zircon, zirconolite, pyrochlore, and brannerite are highly resistant to dissolution. As described above, the alteration of perovskite to anatase and other phases in natural systems is well known [91,93,95–97]. These results are consistent with the available thermodynamic database [94] and are generally corroborated by laboratory experiments carried out over the previous 20 yr on single phase materials and polyphase samples (Synroc-C, etc.). Most of these experiments have been executed at temperatures of 70–150°C in deionized water, sodium chloride, bicarbonate, or silicate solutions, with only a few experiments performed at higher temperatures. Results of these studies indicate that perovskite is the least durable of the major Synroc phases and reacts with aqueous solutions to form an amorphous Ti–O–H film at temperatures below about 100°C or TiO_2 polymorphs (anatase, brookite) at higher temperatures. In contrast, zirconolite generally shows no evidence of alteration at these temperatures, even for experiments lasting up to 532 days [154–162].

Brannerite, pyrochlore, zirconolite, and zircon, on the other hand, are all known to survive the complete destruction of their host rocks during weathering. For example, metamict brannerite samples from Idaho occur in a placer deposit and have survived with minimal dissolution of the original crystals [101]. Pyrochlores are also known to survive weathering and breakdown of their host rocks and, in some carbonatite complexes, the crystals are concentrated to ore grade in the overlying laterite deposits [60,62–64]. Some of these deposits are associated with carbonatite intrusions in Brazil and formed under similar conditions to those where perovskite dissolved [95,96]. The durability of zirconolite is borne out by the occurrence of completely metamict samples in the gem gravel deposits of Sri Lanka [32,81], and there are numerous descriptions of the occurrence of zircon in residual deposits at the earth's surface.

Nevertheless, these phases are susceptible to chemical alteration in certain geological environments. Although generally highly resistant to dissolution, brannerite is susceptible to chemical alteration by ion exchange with the fluid phase and typically loses U while incorporating Si from the fluid phase in the process [101]. Previous work has shown that pyrochlore may exhibit chemical

alteration characterized by various ion exchange effects as a function of temperature and fluid composition. Altered pyrochlores are typically hydrated, but there is only limited evidence for loss of Th and U [58–65]. There are two factors that play a major role in the retention of actinides in pyrochlore structure types. Firstly, Lumpkin and co-workers [59–61] have shown that the ion exchange effects occurring at lower temperatures are generally controlled by the valence of the A-site cation and Y-site anion. Local charge balance constraints tend to limit the leaching to charge balanced A–Y pairs, e.g., Na–F and Ca–O. Therefore, to a first approximation, cation leachability decreases in the order Na > Ca > REE ≫ ACT. Secondly, the geometry of the A-site in pyrochlore closely resembles that of the uranyl (Ur) group in an eight-coordinated $Ur\phi_6$ polyhedron [163], with six short equitorial A–X bonds and two long A–Y axial bonds [45,120]. Numerous chemical analyses of pyrochlore exist which demonstrate the oxidation state of U can range from 100% U^{4+} to 95% U^{6+}. Many of these examples have been altered with no appreciable loss of U (e.g., see [45]), pointing to the inherent stability of U^{6+} in a $Ur\phi_6$-like geometry in pyrochlore.

In contrast, chemical alteration of natural zirconolite is relatively uncommon and the Th and U contents remain more or less constant [32,80,115]. Even though pyrochlore and zirconolite are both derivatives of the fluorite structure type, there is a remarkable difference in the behavior of the minerals in aqueous fluids. Zirconolite can be viewed as a volumetrically condensed, layered version of pyrochlore [38] without the three-dimensional A–Y network. Consequently, there are no tunnels to facilitate ion exchange in zirconolite. Most of the observed alteration effects are representative of high temperature metamorphic or late stage hydrothermal processes. Recent experimental work has confirmed that zirconolite is highly durable in hydrothermal fluids, with some corrosion observed at temperatures of 250–400°C in acidic (up to 0.1 M HCl) or basic (up to 0.1 M NaOH) fluids. Extensive corrosion is only observed at temperatures of about 500°C or higher in these fluids [164,165].

Although zircon is generally considered to be highly durable, we have noted several instances of alteration in this paper, mainly at moderate to high temperatures. From work in progress at ANSTO, it is also apparent that metamict zircon is more susceptible to alteration and may lose a significant amount of U under certain conditions in natural systems (see Fig. 9 and Section 3.5). Previous experimental work has shown that zircon is unstable in NaCl-rich or acidic aqueous fluids at 400–600°C [166,167], in alkaline aqueous fluids at 400°C [168], and in acidic fluids with substantial Cl contents at low temperatures [169]. The forward dissolution rate of zircon has been determined at 120–250°C. Based on the release rate of Si, the dissolution rate of zircon decreases from 4.1×10^{-4} g m^{-2} d^{-1} at 250°C to 1.7×10^{-4} g m^{-2} d^{-1} at 120°C [170]. At ambient temperatures in the laboratory, the dissolution rate of zircon is extremely low [171,172], but the dissolution rate appears to increase by a factor of 60 as the dose increases from 10^{13} (crystalline zircon) to 10^{16} α mg^{-1} (metamict zircon) [172].

The information presented above demonstrates that the highly durable titanate and silicate minerals all exhibit some form of alteration and can be ranked in the following order based on the decreasing magnitude of U loss: brannerite > pyrochlore ⩾ zircon ⩾ zirconolite. This qualitative ranking is consistent with the experimental evidence cited above, and with the latest laboratory test results for brannerite, pyrochlore, zirconolite, and related phases [173–175].

5.2. Alpha-decay damage effects

The mineralogical studies have proven to be quite useful in the area of radiation damage, providing quantitative data on the crystalline–amorphous transformation and the structure of the metamict state. This is especially true in view of the development of AEM procedures for accurate chemical analysis of small volumes (cubic micrometer scale or less) of complex oxide materials and recent advances in knowledge about the thermal histories of some of the important sample localities. In fact, most of the detailed TEM results describing microstructural changes during the crystalline–amorphous transformation due to alpha-decay damage have come from studies of natural samples [114,130,137]. These studies indicate that the titanate and silicate phases of interest become amorphous as a result of the gradual accumulation of alpha-recoil collision cascades which overlap to produce progressively larger amorphous domains until the material becomes aperiodic. Detailed XRD investigations have accompanied some of this work, providing important data on the mass or volume of material damaged per alpha-decay event, unit cell expansion, strain, and crystallite dimensions. These studies have also played a major role in the development of models of damage accumulation (e.g., single impact, double overlap, etc.).

Fig. 22 summarizes the available data in terms of the critical amorphization dose. When extrapolated to short time periods (10 yr or less), the dose curves for pyrochlore, zirconolite, and zircon indicate critical dose values of approximately 1.4×10^{16}, 0.9×10^{16}, and 0.4×10^{16} α mg^{-1}, respectively [115,131]. A comparison with laboratory studies of pyrochlore and zirconolite doped with ^{238}Pu and ^{244}Cm [176–180] shows that the critical dose values of natural pyrochlore and zirconolite are higher by a factor of approximately 2–4. Lumpkin et al. [133] have suggested that this result is due to the long-term storage of the samples in their host rocks

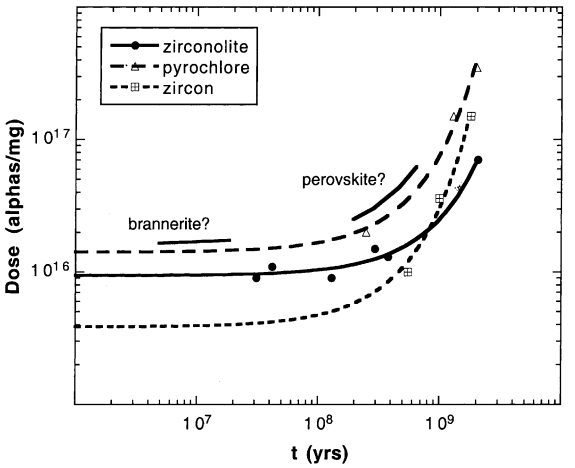

Fig. 22. A summary of the available dose-age data for pyrochlore, zirconolite, zircon, brannerite, and perovskite. Compared with experimental data ($D_c = 0.3$–$0.4 \times 10 \times 10^{16}$ α mg^1), the critical dose curves indicate some recovery of damage in zirconolite and pyrochlore under geological conditions (average $T \sim 100$–200°C). The position of the perovskite dose curve is estimated using data for the onset dose.

at average effective temperatures of 100–200°C, a proposal that is entirely consistent with the available laboratory data for samples that have been stored at elevated temperatures. For example, Clinard et al. [178,180] carried out an important study of $CaPuTi_2O_7$ stored at ambient temperature, 302°C and 602°C. The authors reported that volume swelling was reduced by about 23% in a sample stored at 302°C and the saturation dose increased by about a factor of 2 (XRD indicated that the amorphization dose increased by approximately 20%). In a similar study of Cm-doped Synroc, Mitamura et al. [181] found that the volume expansion was reduced by a factor 2–3 for a sample held at 200°C.

The zircon data shown in Fig. 22 actually indicate a lower short-term critical dose than the experimental data for synthetic zircon samples doped with ^{238}Pu. For example, Weber and co-workers [146,147] report a D_c value of 0.67×10^{16} α mg^{-1} using XRD. The reason for this discrepancy may be due to the limited data set for the natural zircons, together with the general lack of information about the thermal histories of these samples. One possibility is that the older suites of zircon samples plotted in Fig. 22 experienced significantly higher temperatures than the youngest suite (the Sri Lanka samples), producing a critical dose curve with too much upward curvature and a low intercept dose.

Dose-age data also provide evidence for the long-term annealing of isolated alpha-recoil collision cascades in pyrochlore, zirconolite, and zircon. Long-term annealing rate constants obtained from the currently available data sets are approximately 1.7×10^{-9}, 1.0×10^{-9}, and 2.1×10^{-9} yr^{-1}, respectively. For perovskite, Lumpkin et al. [133] have determined a value of 2.1×10^{-9} yr^{-1} using a limited data set for the onset dose. These data indicate that the critical long-term annealing rates of the natural samples are within a factor of about 2 of each other under the geological conditions described above.

5.3. Comparison with heavy ion irradiation data

Considering that the natural samples have different structures, vary dramatically in composition, and have experienced different thermal histories, the results illustrated in Fig. 22 are remarkably consistent. The same structure types have also been studied using 1.0–1.5 MeV Kr ions primarily on thin TEM samples at room temperature [150,182–191]. Results of the ion irradiation experiments indicate that the D_c values of brannerite, pyrochlore, zirconolite, and zircon vary by a factor of about 6, ranging from 0.9×10^{14} ions cm^{-2} up to 6.1×10^{14} ions cm^2. Perovskite tends to amorphize at even higher doses ranging from 3×10^{14} to 18×10^{14} ions cm^{-2} depending on composition and vacancy content [182,187]. When converted to a common unit of dose (e.g., dpa), the ion irradiation data are qualitatively consistent with the results obtained from natural samples and actinide doped samples.

The temperature dependence of the critical amorphization dose determined in some of the ion irradiation studies also indicates that annealing of damage is minimal below temperatures of about 300–400°C. Large differences in the critical temperature (T_c) above which amorphization cannot occur have also been observed in the irradiation experiments. Under similar irradiation conditions, the T_c for zircon is close to 800°C; whereas, values as low as approximately 300°C have been reported for certain zirconolite compositions. These differences in T_c provide a possible explanation for the lower D_c of natural zircon shown in Fig. 22.

In spite of the similarities noted above, there may be fundamental differences in the physics of radiation damage between alpha-decay in bulk materials and ion beam irradiation of thin films. Using plots of $\ln(1 - D_0/D_c)$ versus $1/kT$, Smith et al. [186] have shown that the irradiation data for zirconolite exhibit complex behavior, with the possibility of various annealing mechanisms and different activation energies. In view of the large surface area available for defect migration and annihilation in thin films, one must question the use of these data for long-term prediction of radiation damage in nuclear wasteforms. These data should be validated against the available information from actinide doping experiments and the natural samples for cases where the thermal histories are known.

6. Conclusion

The data summarized in this paper indicate that dedicated petrographic examination and chemical analyses can shed light on the geochemical alteration mechanisms and, in some cases, the P-T-X conditions under which they occur. In support of these studies, there is also a growing body of information relating to the thermodynamic stability and phase relations of minerals like perovskite and zirconolite in the system $CaO–SiO_2–TiO_2–ZrO_2–CO_2$. Furthermore, the incorporation of significant amounts of actinides provides the investigator with a means of studying the alpha-decay damage effects. In fact, this is the only direct way of examining alpha-decay damage apart from actinide doping experiments and is *the only direct means of studying the long-term behavior*. Furthermore, with sufficient geological information, it is now possible in certain cases to estimate the thermal history of the natural samples, providing critical data on the annealing behavior over time.

In closing, it is the opinion of this author that the mineralogical studies have not reached their full potential as a complementary approach to the short-term laboratory based wasteform studies. Today, we clearly have an excellent grasp of the limitations as well as a basic (and growing) knowledge of the fundamental applications of actinide host phases in natural systems. Although a few small groups have achieved much over the past 20 yr, we now have the tools necessary to obtain quantitative data on the crystal chemistry, geochemical alteration, and radiation damage effects. Some specific areas that should be addressed in future work include the following:

- detailed studies of the alteration of natural zircon and thorite;
- modeling of the thermal histories of the host rocks that contain the actinide-bearing minerals;
- quantitative data on temperature, pressure, and fluid composition for specific localities;
- determination of dissolution rates from age dating of weathered deposits;
- an assessment of the relationships between amorphization and geochemical alteration.

Acknowledgements

Over the previous 17 yr, I have had the pleasure of working with numerous individuals on research topics related to the development and testing of nuclear wasteforms and studies of their mineral analogues. In particular I would like to thank R.C. Ewing, B.C. Chakoumakos, K.L. Smith, R. Gieré, and C.T. Williams for their many contributions to various projects. Technical support and expertise for these projects were largely due to the efforts of G. Conrad, K. Kietzke, S. Keyser, M.G. Blackford, M. Colella, R.A. Day, and S. Leung. Further thanks are due to the many museum curators and individuals who have contributed samples for research, including A. Voileau, R.G. Middleton, C.A. Francis, G. Harlow, A.N. Mariano, A.E. Ringwood, S.E. Kesson, and J.S. White.

References

[1] R.C. Ewing, W.J. Weber, F.W. Clinard Jr., Progr. Nucl. Energy 29 (1995) 63.
[2] W.J. Weber, R.C. Ewing, C.R.A. Catlow, T.D. de la Rubia, L.W. Hobbs, C. Kinoshita, Hj. Matzke, A.T. Motta, M. Nastasi, E.K.H. Salje, E.R. Vance, S.J. Zinkle, J. Mater. Res. 13 (1998) 1434.
[3] W. Stoll, Mater. Res. Soc. Bull. 23 (1998) 6.
[4] L.H. Johnson, D.W. Shoesmith, in: W. Lutze, R.C. Ewing (Eds.), Radioactive Waste Forms for the Future, North-Holland, Amsterdam, 1988, p. 635.
[5] W. Lutze, in: W. Lutze, R.C. Ewing (Eds.), Radioactive Waste Forms for the Future, North-Holland, Amsterdam, 1988, p. 1.
[6] A.E. Ringwood, S.E. Kesson, K.D. Reeve, D.M. Levins, E.J. Ramm, in: W. Lutze, R.C. Ewing (Eds.), Radioactive Waste Forms for the Future, North-Holland, Amsterdam, 1988, p. 233.
[7] A.B. Harker, in: W. Lutze, R.C. Ewing (Eds.), Radioactive Waste Forms for the Future, North-Holland, Amsterdam, 1988, p. 335.
[8] E.R. Vance, Mater. Res. Soc. Bull. 19 (1994) 28.
[9] R.L. Garwin, in: W.M. Murphy, D.A. Knecht (Eds.), Scientific Basis for Nuclear Waste Management XIX, Mater. Res. Soc. Symp. Proc., vol. 412, 1996, p. 3.
[10] C. Degueldre, U. Kasemeyer, F. Botta, G. Lederberger, in: W.M. Murphy, D.A. Knecht (Eds.), Scientific Basis for Nuclear Waste Management XIX, Mater. Res. Soc. Symp. Proc., vol. 412, 1996, p. 15.
[11] V.M. Oversby, C.C. McPheeters, C. Degueldre, J.M. Paratte, J. Nucl. Mater. 245 (1997) 17.
[12] B.R. Myers, G.A. Armantrout, C.M. Jantzen, A. Jostsons, J.M. McKibben, H.F. Shaw, D.M. Strachan, J.D. Vienna, Technical Evaluation Panel Summary Report, Plutonium Immobilization Project, Report No. UCRL-ID-129315, 1998.
[13] R.C. Ewing, B.C. Chakoumakos, G.R. Lumpkin, T. Murakami, Mater. Res. Soc. Bull. 12 (1987) 58.
[14] R.C. Ewing, B.C. Chakoumakos, G.R. Lumpkin, T. Murakami, R.B. Greegor, F.W. Lytle, Nucl. Instr. and Meth. B 32 (1988) 487.
[15] R.C. Ewing, Nucl. Instr. and Meth. B 91 (1994) 22.
[16] R.C. Ewing, in: L.A. Kovach, W.M. Murphy (Eds.), Workshop on the Role of Natural Analogs in Geologic Disposal of High-Level Nuclear Waste, NUREG/CP-0147, 1995, p. 29.
[17] R.C. Ewing, Science 286 (1999) 415.
[18] K.P. Hart, G.R. Lumpkin, R. Gieré, C.T. Williams, P.J. McGlinn, T.E. Payne, Radiochim. Acta 74 (1996) 309.

[19] R.C. Ewing, W. Lutze, W.J. Weber, J. Mater. Res. 10 (1995) 243.
[20] R.C. Ewing, Proc. Natl. Acad. Sci. USA 96 (1999) 3432.
[21] G.R. Lumpkin, J. Nucl. Mater. 274 (1999) 206.
[22] A. Pabst, Am. Mineral. 37 (1952) 137.
[23] P.M. Hurley, H.W. Fairbairn, Geol. Soc. Am. Bull. 64 (1953) 659.
[24] H.D. Holland, D. Gottfried, Acta Crystallogr. 8 (1955) 291.
[25] G.J. McCarthy, Nucl. Technol. 32 (1977) 92.
[26] R. Roy, J. Am. Ceram. Soc. 60 (1977) 350.
[27] A.E. Ringwood, Safe Disposal of High Level Nuclear Reactor Wastes: A New Strategy, Australian National University Press, Canberra, 1978.
[28] A.E. Ringwood, S.E. Kesson, N.G. Ware, W. Hibberson, A. Major, Nature 278 (1979) 219.
[29] A.E. Ringwood, S.E. Kesson, N.G. Ware, W. Hibberson, A. Major, Geochem. J. 13 (1979) 141.
[30] A.E. Ringwood, V.M. Oversby, S.E. Kesson, W. Sinclair, N.G. Ware, W. Hibberson, A. Major, Nucl. Chem. Waste Manage. 2 (1981) 287.
[31] W. Sinclair, A.E. Ringwood, Geochem. J. 15 (1981) 229.
[32] V.M Oversby, A.E. Ringwood, Rad. Waste Manage. 1 (1981) 289.
[33] R.C. Ewing, Science 192 (1976) 1336.
[34] R.C. Ewing, R.F. Haaker, Nucl. Chem. Waste Manage. 1 (1980) 51.
[35] R.F. Haaker, R.C. Ewing, in: C.J.M. Northrup (Ed.), Scientific Basis for Nuclear Waste Management II, Plenum, New York, 1980, p. 281.
[36] M.A. Subramanian, G. Aravamudan, G.V. Subba Rao, Prog. Solid State Chem. 15 (1983) 55.
[37] B.C. Chakoumakos, J. Solid State Chem. 53 (1984) 120.
[38] K.L. Smith, G.R. Lumpkin, in: J.N. Boland, J.D. Fitz Gerald (Eds.), Defects and Processes in the Solid State: Geoscience Applications, the McLaren Volume, Elsevier, Amsterdam, 1993, p. 401.
[39] R.D. Shannon, Acta Crytallogr. A 32 (1976) 751.
[40] D.D. Hogarth, Can. Mineral. 6 (1961) 610.
[41] G. Perrault, Can. Mineral. 9 (1968) 383.
[42] W. Petruk, D.R. Owens, Can. Mineral. 13 (1975) 282.
[43] D.D. Hogarth, Am. Mineral. 62 (1977) 403.
[44] O. Von Knorring, A. Fadipe, Bull. Soc. Fr. Minéal. Cristallogr. 104 (1981) 496.
[45] G.R. Lumpkin, B.C. Chakoumakos, R.C. Ewing, Am. Mineral. 71 (1986) 569.
[46] M.A. Wise, P. Cerny, Mineral. Petrol. 43 (1990) 83.
[47] N.A. Hodgson, M.J. Le Bas, Mineral. Mag. 56 (1992) 201.
[48] D. Ohnenstetter, P. Piantone, Can. Mineral. 30 (1992) 771.
[49] B.C. Chakoumakos, R.C. Ewing, in: C.M. Jantzen, J.A. Stone, R.C. Ewing (Eds.), Scientific Basis for Nuclear Waste Management VIII, Mater. Res. Soc. Symp. Proc., vol. 44, 1985, p. 641.
[50] T.S. Ercit, F.C. Hawthorne, P. Cerny, Can. Mineral. 32 (1994) 415.
[51] E. Jäger, E. Niggli, A.H. van der Veen, Mineral. Mag. 32 (1959) 10.
[52] A.H. vander Veen, Verhandelingen van het Koninklijk Nederlands geologisch mijnbouwkundig genootschap, Geologische serie, 22, 1963.
[53] P.M. Harris, Mineral. Mag. 35 (1965) 277.
[54] L. Van Wambeke, Mineral. Deposita 6 (1971) 153.
[55] L. Van Wambeke, Am. Mineral. 63 (1978) 528.
[56] L. Van ambeke, N. Jarhb. ineral. Abh. 112 (1970) 117.
[57] R.C. Ewing, Geochim. Cosmochim. Acta 39 (1975) 521.
[58] G.R. Lumpkin, R.C. Ewing, in: C.M. Jantzen, J.A. Stone, R.C. Ewing (Eds.), Scientific Basis for Nuclear Waste Management VIII, Mater. Res. Soc. Symp. Proc., vol. 44, 1985, p. 647.
[59] G.R. Lumpkin, R.C. Ewing, Am. Mineral. 77 (1992) 179.
[60] G.R. Lumpkin, R.C. Ewing, Am. Mineral. 80 (1995) 732.
[61] G.R. Lumpkin, R.C. Ewing, Am. Mineral. 81 (1996) 1237.
[62] G.R. Lumpkin, A.N. Mariano, in: W.M. Murphy, D.A. Knecht (Eds.), Scientific Basis for Nuclear Waste Management XIX, Mater. Res. Soc. Symp. Proc., vol. 412, 1996, p. 831.
[63] A.N. Mariano, G.R. Lumpkin, S.H.F. Leung, Presented at the Geological Association of Canada/Mineralogical Association of Canada Annual Meeting, Ottawa, Canada, 1997, Abstracts, vol. 22, p. A-97.
[64] F. Wall, C.T. Williams, A.R. Woolley, M. Nasraoui, Mineral. Mag. 60 (1996) 731.
[65] G.R. Lumpkin, R.A. Day, P.J. McGlinn, T.E. Payne, R. Gieré, C.T. Williams, in: D.J. Wronkiewicz, J.H. Lee (Eds.), Scientific Basis for Nuclear Waste anagement XXII, Mater. Res. Soc. Symp. Proc., vol. 556, 1999, p. 793.
[66] B.M. Gatehouse, I.E. Grey, R.J. Hill, H.J. Rossell, Acta Crystallogr. B 37 (1981) 306.
[67] H.J. Rossell, J. Solid State Chem. 99 (1992) 38.
[68] H.J. Rossell, J. Solid State Chem. 99 (1992) 52.
[69] W. Sinclair, R.A. Eggleton, Am. Mineral. 67 (1982) 615.
[70] P.E. Fielding, T.J. White, J. Mater. Res. 2 (1987) 387.
[71] M.B. Fowler, C.T. Williams, Mineral. Mag. 50 (1986) 326.
[72] R.G. Platt, F. Wall, C.T. Williams, A.R. Woolley, Mineral. Mag. 51 (1987) 253.
[73] C.T. Williams, R. Gieré, Schweiz. Mineral. Petrogr. Mitt. 68 (1988) 133.
[74] R. Gieré, C.T. Williams, Contrib. Mineral. Petrol. 112 (1992) 83.
[75] S.L. Harley, Mineral. Mag. 58 (1994) 259.
[76] A.G. Bulakh, A.R. Nesterov, C.T. Williams, I.S. Anisimov, Mineral. Mag. 62 (1998) 837.
[77] F. Bellatreccia, G. Della Ventura, E. Caprilli, C.T. Williams, G.C. Parodi, Mineral. Mag. 63 (1999) 649.
[78] C.T. Williams, R. Gieré, Bull. Nat. Hist. Mus. Lond. (Geol.) 52 (1996) 1.
[79] R. Gieré, C.T. Williams, G.R. Lumpkin, Schweiz. Mineral. Petrogr. Mitt. 78 (1998) 433.
[80] R.C. Ewing, R.F. Haaker, T.J. Headley, P.F. Hlava, in: S.V. Topp (Ed.), Scientific Basis for Nuclear Waste Management VI, Elsevier, New York, 1982, p. 249.
[81] T.E. Payne, G.R. Lumpkin, P.J. McGlinn, K.P. Hart, in: T. Murakami, R.C. Ewing (Eds.), Scientific Basis for Nuclear Waste Management XVIII, Mater. Res. Soc. Symp. Proc., vol. 353, 1995, p. 1259.
[82] Y. Pan, Can. Mineral. 35 (1997) 105.
[83] G.R. Lumpkin, K.P. Hart, P.J. McGlinn, T.E. Payne, R. Gieré, C.T. Williams, Radiochim. Acta 66&67 (1994) 469.
[84] R. Gieré, R. Guggenheim, M. Düggelin, D. Mathys, C.T. Williams, G.R. Lumpkin, K.L. Smith, M.G. Blackford, K.P. Hart, P. McGlinn, in: Proceedings of the 13th

International Congress on Electron Microscopy, Applications in Materials Sciences, vol. 2B, 1994, p. 1269.
[85] R.H. Mitchell, in: A.P. Jones, F. Wall, C.T. Williams (Eds.), Rare Earth Minerals, Chemistry, Origin and Ore Deposits, Chapman & Hall, London, 1996, p. 41.
[86] S.E. Haggerty, A.N. Mariano, Contrib. Mineral. Petrol. 84 (1983) 365.
[87] R.H. Mitchell, I.M. Steele, Can. Mineral. 30 (1992) 1153.
[88] R.H. Mitchell, N.V. Vladykin, Mineral. Mag. 57 (1993) 651.
[89] R.H. Mitchell, A.R. Chakhmouradian, Mineral. Mag. 62 (1998) 341.
[90] A.R. Chakhmouradian, R.H. Mitchell, Mineral. Mag. 62 (1998) 769.
[91] R.H. Mitchell, A.R. Chakhmouradian, Can. Mineral. 36 (1998) 939.
[92] A.R. Chakhmouradian, R.H. Mitchell, Can. Mineral. 36 (1998) 953.
[93] A.R. Chakhmouradian, R.H. Mitchell, A.V. Pankov, N.V. Chukanov, Mineral. Mag. 63 (1999) 519.
[94] H.W. Nesbitt, G.M. Bancroft, W.S. Fyfe, S.N. Karkhanis, A. Nishijima, S. Shin, Nature 289 (1981) 358.
[95] A.N. Mariano, in: B.R. Lipin, G.A. McKay (Eds.), Geochemistry and Mineralogy of Rare Earth Elements, Reviews in Mineralogy, vol. 21, Mineralogical Society of America, Washington, DC, 1989, p. 309.
[96] J.F. Banfield, D.R. Veblen, Am. Mineral. 77 (1992) 545.
[97] R.L. Erickson, L.V. Blade, US Geol. Surv. Prof. Pap. 425 (1963).
[98] G.R. Lumpkin, M. Colella, K.L. Smith, R.G. Mitchell, A.O. Larsen, in: I.G. McKinley, C. McCombie (Eds.), Scientific Basis for Nuclear Waste Management XXI, Mater. Res. Soc. Symp. Proc., vol. 506, 1998, p. 207.
[99] J.T. Szymanski, J.D. Scott, Can. Mineral. 20 (1982) 271.
[100] E.R. Vance, J.N. Watson, M.L. Carter, R.A. Day, G.R. Lumpkin, K.P. Hart, Y. Zhang, P.J. McGlinn, M.W.A. Stewart, D.J. Cassidy, Cer. Trans. 107 (2000) 561.
[101] G.R. Lumpkin, S.H.F. Leung, M. Colella, in: R.W. Smith, D.W. Shoesmith (Eds.), Scientific Basis for Nuclear Waste Management XXIII, Mater. Res. Soc. Symp. Proc., vol. 608, 2000, p. 359.
[102] A. Pabst, Am. Mineral. 39 (1954) 109.
[103] F. Bianconi, A. Simonetti, Schweiz. Mineral. Petrogr. Mitt. 47 (1967) 887.
[104] M. Fleischer, G.Y. Chao, J.A. Mandarino, Am. Mineral. 64 (1979) 652.
[105] J.A. Speer, in: P.H. Ribbe (Ed.), Orthosilicates, Reviews in Mineralogy, second ed., vol. 5, Mineralogical Society of America, Washington, DC, 1982, p. 67.
[106] R.D. Aines, G.R. Rossman, Am. Mineral. 71 (1986) 1186.
[107] J.N. Rubin, C.D. Henry, J.G. Price, Am. Mineral. 74 (1989) 865.
[108] D.M. Wayne, A.K. Sinha, D.A. Hewitt, Contrib. Mineral. Petrol. 109 (1992) 408.
[109] D. Carroll, J. Sed. Petrol. 23 (1953) 106.
[110] D.M. Wayne, A.K. Sinha, Contrib. Mineral. Petrol. 98 (1988) 109.
[111] R. Törnroos, Bull. Geol. Soc. Finland 57 (1985) 181.
[112] G.K. Krivokoneva, G.A. Sidorenko, Geochem. Int. 8 (1971) 113.
[113] G.R. Lumpkin, E.M. Foltyn, R.C. Ewing, J. Nucl. Mater. 129 (1986) 113.
[114] G.R. Lumpkin, R.C. Ewing, Phys. Chem. Minerals 16 (1988) 2.
[115] G.R. Lumpkin, K.P. Hart, P.J. McGlinn, T.E. Payne, R. Gieré, C.T. Williams, Radiochim. Acta 66&67 (1994) 469.
[116] Y. Eyal, R.L. Fleischer, Geochim. Cosmochim. Acta 49 (1985) 1155.
[117] Y. Eyal, G.R. Lumpkin, R.C. Ewing, in: L.O. Werme (Ed.), Scientific Basis for Nuclear Waste Management IX, Mater. Res. Soc. Symp. Proc., vol. 50, 1985, p. 379.
[118] Y. Eyal, G.R. Lumpkin, R.C. Ewing, in: J.K. Bates, W.B. Seefeldt (Eds.), Scientific Basis for Nuclear Waste Management X, Mater. Res. Soc. Symp. Proc., vol. 84, 1987, p. 635.
[119] G.R. Lumpkin, R.C. Ewing, Y. Eyal, J. Mater. Res. 3 (1988) 357.
[120] R.B. Greegor, F.W. Lytle, B.C. Chakoumakos, G.R. Lumpkin, R.C. Ewing, in: C.M. Jantzen, J.A. Stone, R.C. Ewing (Eds.), Scientific Basis for Nuclear Waste Management VIII, Mater. Res. Soc. Symp. Proc., vol. 44, 1985, p. 655.
[121] R.B. Greegor, F.W. Lytle, B.C. Chakoumakos, G.R. Lumpkin, R.C. Ewing, in: L.O. Werme (Ed.), Scientific Basis for Nuclear Waste Management IX, Mater. Res. Soc. Symp. Proc., vol. 50, 1985, p. 387.
[122] R.B. Greegor, F.W. Lytle, B.C. Chakoumakos, G.R. Lumpkin, R.C. Ewing, C.L. Spiro, J. Wong, in: J.K. Bates, W.B. Seefeldt (Eds.), Scientific Basis for Nuclear Waste Management X, Mater. Res. Soc. Symp. Proc., vol. 84, 1987, p. 645.
[123] R.B. Greegor, F.W. Lytle, B.C. Chakoumakos, G.R. Lumpkin, J.K. Warner, R.C. Ewing, in: W. Lutze, R.C. Ewing (Eds.), Scientific Basis for Nuclear Waste Management XII, Mater. Res. Soc. Symp. Proc., vol. 127, 1989, p. 261.
[124] R.C. Ewing, T.J. Headley, J. Nucl. Mater. 119 (1983) 102.
[125] G.R. Lumpkin, R.C. Ewing, B.C. Chakoumakos, R.B. Greegor, F.W. Lytle, E.M. Foltyn, F.W. Clinard Jr., L.A. Boatner, M.M. Abraham, J. Mater. Res. 1 (1986) 564.
[126] R.B. Greegor, F.W. Lytle, R.C. Ewing, R.F. Haaker, Nucl. Instr. and Meth. B 1 (1984) 587.
[127] F. Farges, R.C. Ewing, G.E. Brown Jr., J. Mater. Res. 8 (1993) 1983.
[128] F. Farges, Am. Mineral. 82 (1997) 44.
[129] G.R. Lumpkin, K.L. Smith, M.G. Blackford, R. Gieré, C.T. Williams, Micron 25 (1994) 581.
[130] G.R. Lumpkin, K.L. Smith, R. Gieré, Micron 28 (1997) 57.
[131] G.R. Lumpkin, K.L. Smith, M.G. Blackford, R. Gieré, C.T. Williams, in: I.G. McKinley, C. McCombie (Eds.), Scientific Basis for Nuclear Waste Management XXI, Mater. Res. Soc. Symp. Proc., vol. 506, 1998, p. 215.
[132] R.A. Van Konynenburg, M.W. Guinan, Nucl. Technol. 60 (1983) 206.
[133] G.R. Lumpkin, M. Colella, K.L. Smith, R.H. Mitchell, A.O. Larsen, in: I.G. McKinley, C. McCombie (Eds.), Scientific Basis for Nuclear Waste Management XXI, Mater. Res. Soc. Symp. Proc., vol. 506, 1998, p. 207.
[134] S. Graeser, R. Guggenheim, Schweiz. Mineral. Petrogr. Mitt. 70 (1990) 325.

[135] I.M. Lipova, G.A. Kuznetsova, Ye.S. Makarov, Geochem. Int. 2 (1965) 513.
[136] T. Murakami, B.C. Chakoumakos, R.C. Ewing, in: D.E. Clark, W.B. White, J. Machiels (Eds.), Advances in Ceramics, Nuclear Waste Management II, vol. 20, American Ceramic Society, Columbus, Ohio, 1986, p. 745.
[137] T. Murakami, B.C. Chakoumakos, R.C. Ewing, G.R. Lumpkin, W.J. Weber, Am. Mineral. 76 (1991) 1510.
[138] C.J. Howard, T.M. Sabine, J. Phys. Chem. 7 (1974) 3453.
[139] L.A. Bursill, A.C. McLaren, Phys. Stat. Solid 13 (1966) 331.
[140] E.R. Vance, B.W. Anderson, Mineral. Mag. 38 (1972) 605.
[141] T.J. Headley, R.C. Ewing, R.F. Haaker, in: G.W. Bailey (Ed.), in: Proceedings of the 39th Annual Proceedings of the Electron Microscopy Society of America, Atlanta, Georgia, 1981, p. 112.
[142] M. Zhang, E.K.H. Salje, I. Farnan, A. Graeme-Barber, P. Daniel, R.C. Ewing, A.M. Clark, H. Leroux, J. Phys. 12 (2000) 1915.
[143] S. Ellsworth, A. Navrotsky, R.C. Ewing, Phys. Chem. Minerals 21 (1994) 140.
[144] B.C. Chakoumakos, T. Murakami, G.R. Lumpkin, R.C. Ewing, Science 236 (1987) 1556.
[145] B.C. Chakoumakos, W.C. Oliver, G.R. Lumpkin, R.C. Ewing, Rad. Eff. Def. Solid 118 (1991) 393.
[146] W.J. Weber, J. Mater. Res. 5 (1990) 2687.
[147] W.J. Weber, Nucl. Instr. and Meth. B 65 (1992) 88.
[148] W.J. Weber, R.C. Ewing, L.M. Wang, J. Mater. Res. 9 (1994) 688.
[149] S. Ríos, E.K.H. Salje, M. Zhang, R.C. Ewing, J. Phys. 12 (2000) 2401.
[150] W.J. Weber, R.C. Ewing, W. Lutze, in: W.M. Murphy, D.A. Knecht (Eds.), Scientific Basis for Nuclear Waste Management XIX, Mater. Res. Soc. Proc., vol. 412, 1996, p. 25.
[151] W.J. Weber, R.C. Ewing, A. Meldrum, J. Nucl. Mater. 250 (1997) 147.
[152] A. Meldrum, L.A. Boatner, W.J. Weber, R.C. Ewing, Geochim. Cosmochim. Acta 62 (1998) 2509.
[153] A. Meldrum, L.A. Boatner, S.J. Zinkle, S.X. Wang, L.M. Wang, R.C. Ewing, Can Mineral. 37 (1999) 207.
[154] T. Kastrissios, M. Stephenson, P.S. Turner, J. Am. Ceram. Soc. 70 (1987) C144.
[155] S. Myhra, H.E. Bishop, J.C. Riviere, M. Stephenson, J. Mater. Sci. 22 (1987) 3217.
[156] S. Myhra, P. Delogu, R. Giorgi, J.C. Riviere, J. Mater. Sci. 23 (1988) 1514.
[157] K.L. Smith, K.P. Hart, G.R. Lumpkin, P. McGlinn, P. Lam, M.G. Blackford, in: T.A. Abrajano Jr., L.A. Johnson (Eds.), Scientific Basis for Nuclear Waste Management XIV, Mater. Res. Soc. Symp. Proc., vol. 212, 1991, p. 167.
[158] G.R. Lumpkin, K.L. Smith, M.G. Blackford, J. Mater. Res. 6 (1991) 2218.
[159] K.L. Smith, G.R. Lumpkin, M.G. Blackford, R.A. Day, K.P. Hart, J. Nucl. Mater. 190 (1992) 287.
[160] P.J. McGlinn, K.P. Hart, E.H. Loi, E.R. Vance, in: T. Murakami, R.C. Ewing (Eds.), Scientific Basis for Nuclear Waste Management XVIII, Mater. Res. Soc. Symp. Proc., vol. 353, 1995, p. 847.
[161] G.R. Lumpkin, K.L. Smith, M.G. Blackford, in: T. Murakami, R.C. Ewing (Eds.), Scientific Basis for Nuclear Waste Management XVIII, Mater. Res. Soc. Symp. Proc., vol. 353, 1995, p. 855.
[162] K.L. Smith, M. Colella, G.J. Thorogood, M.G. Blackford, G.R. Lumpkin, K.P. Hart, K. Prince, E. Loi, A. Jostsons, in: W.J. Gray, I.R. Triay (Eds.), Scientific Basis for Nuclear Waste Management XX, Mater. Res. Soc. Symp. Proc., vol. 465, 1997, p. 349.
[163] P.C. Burns, R.C. Ewing, M.L. Miller, J. Nucl. Mater. 245 (1997) 1.
[164] J. Malmström, E. Reusser, R. Gieré, G.R. Lumpkin, M. Düggelin, D. Mathys, R. Guggenheim, in: D.J. Wronkiewicz, J.H. Lee (Eds.), Scientific Basis for Nuclear Waste Management XXII, Mater. Res. Soc. Symp. Proc., vol. 556, 1999, p. 165.
[165] J. Malmström, E. Reusser, R. Gieré, G.R. Lumpkin, M.G. Blackford, M. Düggelin, D. Mathys, R. Guggenheim, D. Günther, in: R.W. Smith, D.W. Shoesmith (Eds.), Scientific Basis for Nuclear Waste Management XXIII, Mater. Res. Soc. Symp. Proc., vol. 608, 2000, p. 475.
[166] R.T. Pidgeon, J.R. O'Neil, L.T. Silver, Science 154 (1966) 1538.
[167] A.K. Sinha, D.M. Wayne, D.A. Hewitt, Geochim. Cosmochim. Acta 56 (1992) 3551.
[168] O.D. Maurice, Econ. Geol. 44 (1949) 721.
[169] F. Colin, C. Alarcon, P. Vieillard, Chem. Geol. 107 (1993) 273.
[170] K.B. Helean, W. Lutze, R.C. Ewing, Ceram. Trans. 93 (1999) 297.
[171] R.C. Ewing, R.F. Haaker, W. Lutze, in: W. Lutze (Ed.), Scientific Basis for Nuclear Waste Management V, Elsevier, New York, 1982, p. 389.
[172] M.P. Tole, Geochim. Cosmochim. Acta 49 (1985) 453.
[173] Y. Zhang, G. Lumpkin, K. Hart, R. Day, in: Proceedings of the Seventh International Conference on the Chemistry and Migration Behavior of Actinides and Fission Products in the Geosphere, Abstracts, Migration '99, Lake Tahoe, NV, 1999, p. 18.
[174] W.L. Bourcier, S.K. Roberts, H.F. Shaw, in: Proceedings of the Seventh International Conference on the Chemistry and Migration Behavior of Actinides and Fission Products in the Geosphere, Abstracts, Migration '99, Lake Tahoe, NV, 1999, p. 32.
[175] K.P. Hart, Y. Zhang, E. Loi, Z. Aly, M.W.A. Stewart, A. Brownscombe, B.B. Ebbinghaus, W. Bourcier, in: R.W. Smith, D.W. Shoesmith (Eds.), Scientific Basis for Nuclear Waste Management XXIII, Mater. Res. Soc. Symp. Proc., vol. 608, 2000, p. 353.
[176] J.W. Wald, P. Offermann, in: W. Lutze (Ed.), Scientific Basis for Nuclear Waste Management V, Elsevier, New York, 1982, p. 369.
[177] F.W. Clinard Jr., D.L. Rohr, R.B. Roof, Nucl. Instr. and Meth. B 1 (1984) 581.
[178] F.W. Clinard Jr., D.E. Peterson, D.L. Rohr, L.W. Hobbs, J. Nucl. Mater. 126 (1984) 245.
[179] W.J. Weber, J.W. Wald, Hj. Matzke, J. Nucl. Mater. 138 (1986) 196.
[180] F.W. Clinard Jr., Ceram. Bull. 65 (1986) 1181.
[181] H. Mitamura, S. Matsumoto, T. Miyazaki, T.J. White, K.Nukaga, Y. Togashi, T. Sagawa, S. Tashiro, D.M. Levins, A. Kikuchi, J. Am. Ceram. Soc. 73 (1990) 3433.

[182] K.L. Smith, N.J. Zaluzec, G.R. Lumpkin, J. Nucl. Mater. 250 (1997) 36.
[183] S.X. Wang, L.M. Wang, R.C. Ewing, G.S. Was, G.R. Lumpkin, Nucl. Instr. and Meth. B 148 (1999) 704.
[184] S.X. Wang, G.R. Lumpkin, L.M. Wang, R.C. Ewing, Nucl. Instr. and Meth. B 166&167 (2000) 293.
[185] S.X. Wang, L.M. Wang, R.C. Ewing, K.V.G. Kutty, Nucl. Instr. and Meth. B 169 (2000) 135.
[186] K.L. Smith, M.G. Blackford, G.R. Lumpkin, N.J. Zaluzec, in: R.W. Smith, D.W. Shoesmith (Eds.), Scientific Basis for Nuclear Waste Management XXIII, Mater. Res. Soc. Symp. Proc., vol. 608, 2000, p. 487.
[187] K.L. Smith, G.R. Lumpkin, M.G. Blackford, E.R. Vance, in: S.J. Zinkle, G.E. Lucas, R.C. Ewing, and J.S. Williams (Eds.), Microstructural Processes in Irradiated Materials, Mater. Res. Soc. Symp. Proc., vol. 540, 1999, p. 323.
[188] K.L. Smith, M.G. Blackford, G.R. Lumpkin, N.J. Zaluzec, J. Nucl. Mater. 277 (2000) 159.
[189] B.D. Begg, W.J. Weber, R. Devanathan, J.P. Icenhower, S. Thevuthasan, B.P. McGrail, Ceram. Trans. 107 (2000) 553.
[190] B.D. Begg, N.J. Hess, D.E. McCready, S. Thevuthasan, W.J. Weber, J. Nucl. Mater., these Proceedings.
[191] G.R. Lumpkin, K.L. Smith, M.G. Blackford, these Proceedings.